Nicolas Chevigny[1], Frédérique Weber-Lotfi[1], Cédric Nadiras[1], Arnaud Fertet[1], Monique Le Ret[1], Marc Bichara[4], Mathieu Erhardt[1], André Dietrich[1], Cécile Raynaud[2,3] and José M. Gualberto[1]

[1]Institut de Biologie Moléculaire des Plantes, CNRS, Université de Strasbourg, 12 rue du General Zimmer, 67084 Strasbourg, France

[2]Université Paris-Saclay, CNRS, INRAE, Univ Evry, Institute of Plant Sciences Paris-Saclay (IPS2), 91405 Orsay, France.

[3]Université de Paris, CNRS, INRAE, Institute of Plant Sciences Paris Saclay (IPS2) 91405 Orsay

[4]Biotechnologie et Signalisation Cellulaire, CNRS, Université de Strasbourg, Bld Sébastien Brandt BP10413, 67412 Illkirch, France

***Corresponding author:**

José M. Gualberto

Institut de Biologie Moléculaire des Plantes, CNRS, Université de Strasbourg
12 rue du General Zimmer, 67084 Strasbourg, France
Tel (+33) 367155361
Fax (+33) 3 67 15 53 00
jose.gualberto@ibmp-cnrs.unistra.fr

Title:

RADA is a main branch migration factor in plant mitochondrial recombination and its defect leads to mtDNA instability and cell cycle arrest

Running title: RADA in mitochondrial genome stability

The author responsible for distribution of materials integral to the findings presented in this article in accordance with the policy described in the Instructions for Authors (www.plantcell.org) is José M. Gualberto (jose.gualberto@ibmp-cnrs.unistra.fr).

SYNOPSIS

RADA is a main branch migration activity in plant mitochondria, whose deficiency leads to mtDNA instability and suppression of plant growth by activation of repressors of cell cycle progression.

ABSTRACT

The mitochondria of flowering plants have large and complex genomes whose structure and segregation are modulated by recombination activities. The late steps of mitochondrial recombination are still poorly characterized: while the loss of mitochondrial recombination is not viable, a deficiency in RECG1-dependent branch migration has little impact on plant development, implying the existence of alternative pathways. Here we present *RADA*, an ortholog of bacterial RadA/Sms, which is required for the processing of organellar recombination intermediates. While bacterial RadA is dispensable, RADA-deficient plants are severely impacted in their development and fertility, correlating with increased mtDNA ectopic recombination and replication of recombination-generated subgenomes. The *radA* mutation is epistatic to *recG1*, indicating that RADA drives the main branch migration pathway of plant mitochondria. In contrast, the double mutation *radA recA3* is lethal, underlining the importance of an alternative RECA3-dependent pathway. Although RADA is dually targeted to mitochondria and chloroplasts, we found little to no effects of *radA* on the stability of the plastidial genome. The stunted growth of *radA* mutants could not be correlated with obvious defects in mitochondrial gene expression. Rather, it seems that is partially caused by a retrograde signal that activates nuclear genes repressing cell cycle progression.

INTRODUCTION

The mitochondrial genomes (mtDNA) of vascular plants are large and complex, mostly consisting of non-coding sequences assembled in a heterogeneous population of linear, circular and branched double-stranded (dsDNA) or single-stranded (ssDNA) DNA molecules (Backert et al., 1997; Bendich, 1996; Manchekar et al., 2006). In most species this collection of subgenomic molecules can be mapped into a single circular chromosome, but multichromosome mitogenomes can also exist (Sloan, 2013). The complexity of the plant mtDNA comes from frequent homologous recombination (HR) events involving repeated sequences. Large repeated sequences (>500 bp) are involved in frequent and reversible HR, while intermediate-size repeats (IRs) (50-500 bp) or microhomologies (<50 bp) can promote infrequent ectopic or illegitimate recombination, respectively (Christensen, 2018; Gualberto et Newton, 2017; Maréchal et Brisson, 2010; Woloszynska et Trojanowski, 2009). Recombination involving IRs or microhomologies contributes to the heteroplasmic state of mtDNA by creating sub-stoichiometric alternative configurations (mitotypes) that co-exist with the main genome (Small et al., 1989). Sub-stoichiometric mtDNA variants can become the predominant genome in the time frame of a single plant generation by a yet unclear process of clonal expansion called sub-stoichiometric shifting (Janska et al., 1998; Small et al., 1989; Vitart et al., 1992). These variants may present altered gene expression, resulting from the displacement of regulatory sequences or from the disruption of gene sequences. Such events may lead to the creation and expression of chimeric ORFs that can be deleterious for mitochondrial function, like in the case of cytoplasmic male sterility (CMS) (Budar et al., 2003; Hanson et Bentolila, 2004). HR is also the main pathway of plant mitochondria for the repair of double strand breaks (DSBs) and the copy-correction of mutations, thus contributing to the very slow evolution of plant mtDNA coding sequences (Christensen, 2013; Mower et al., 2007).

Defect in the factors involved in plant organellar recombination pathways can cause genomic rearrangements, because of increased ectopic recombination resulting from the activation of alternative error-prone repair pathways (Miller-Messmer et al., 2012; Wallet et al., 2015). Many of these factors are derived from prokaryotic homologs inherited from the symbiotic ancestors of mitochondria and chloroplasts (Boesch et al., 2011; Gualberto et Newton, 2017). However, the organellar pathways can significantly depart from thouse of their bacterial counterparts, and involve additional factors with partially redundant functions. As a representative example, plant organellar recombination relies on the abundant RecA-like RECA2 recombinase [(about 450 copies/mitochondrion (Fuchs et al., 2019)], which is targeted to both organelles and whose mutation is lethal at the seedling developmental stage (Miller-Messmer et al., 2012; Shedge et al., 2007). But this process also involves plastidial

101 RECA1 and mitochondrial RECA3. RECA3 could not be detected in Arabidopsis cultured
102 cells (Fuchs et al., 2019), but its function is critical for mtDNA maintenance, since its loss
103 causes mtDNA instability that worsens over generations (Miller-Messmer et al., 2012;
104 Shedge et al., 2007). Double mutants of *RECA3* and other mitochondrial recombination
105 factors such as MSH1 and RECG1 are also much more affected in development than the
106 individual homozygote mutants (Shedge et al., 2007; Wallet et al., 2015). This apparently
107 reflects specialized functions and RECA3-dependant alternative recombination pathways,
108 maybe because *RECA3* is expressed in specific tissues such as pollen and ovules (Miller-
109 Messmer et al., 2012). It was also recently found that tobacco *RECA3* is cell cycle regulated
110 (Trolet et al., 2019).

111 In bacteria, HR is initiated by the loading of RecA on ssDNA, forming a nucleofilament
112 that then seeks for homologies in the genome by probing multiple heterologous sequences
113 (Forget et Kowalczykowski, 2012; Ragunathan et al., 2012). When a homologous sequence
114 is identified, RecA-mediated ATP hydrolysis stabilizes the invading DNA, forming the
115 synaptic complex also known as displacement loop or D-loop. An important post-synaptic
116 step is branch migration, which involves helicases that extend the homologous region on
117 both sides of the D-loop, allowing the recruitment of the fourth DNA strand to form a Holliday
118 Junction (Cooper et Lovett, 2016; West, 1997; Whitby et al., 1994). Three partially redundant
119 pathways of branch migration have been described in bacteria, involving RuvAB, RecG and
120 RadA, respectively (Beam et al., 2002; Cooper et al., 2015). RadA (also known as "Sms" for
121 "sensitivity to methylmethane sulfonate" and not to be confused with Archea RadA that is
122 unrelated) has long been known as a factor influencing repair by recombination (Beam et al.,
123 2002; Slade et al., 2009), but its biochemical activities were only recently characterized
124 (Cooper et Lovett, 2016; Marie et al., 2017). It is an ATP-dependent ssDNA helicase
125 composed of three functional domains: an N-terminal C4 zinc-finger, a RecA-like ATPase
126 domain and a Lon protease-like domain (Cooper et al., 2015). In contrast to RecG and
127 RuvAB, RadA interacts with RecA and can function in the context of the RecA
128 nucleofilament. Bacterial *radA* or *recG* single mutants are only mildly affected in DNA repair,
129 but the *radA recG* double mutant is severely impaired in its survival under genotoxic
130 conditions (Cooper et al., 2015). Highlighting the crucial role of branch migration in HR, the
131 deficiency in multiple branch migration pathways is more deleterious to the cell than the
132 absence of recombination, because of the accumulation of toxic unprocessed intermediates
133 (Beam et al., 2002; Cooper et al., 2015).

134 In Arabidopsis mitochondria, RECA-dependent recombination is apparently essential,
135 because *recA2 recA3* double mutants could not be obtained (Miller-Messmer et al., 2012).
136 Plant genomes do not encode any homolog of the RuvAB branch migration complex, but
137 code for an organellar-targeted RecG homolog (RECG1) (Odahara et al., 2015; Wallet et al.,

138 2015). But despite of the absence of a mitochondrial RuvAB pathway, *recG1* mutants are
139 only mildly affected in development. Since mitochondrial HR is apparently essential, a more
140 deleterious effect was expected for the loss of this branch migration activity, suggesting the
141 existence of additional pathways for the maturation of recombination intermediates.
142 Here we describe a plant homolog to eubacterial RadA/Sms, which could potentially
143 be involved in the late steps of organellar HR pathways. We show that Arabidopsis RADA
144 possesses similar activities as bacterial RadA. However, contrarily to bacteria, plant *radA*
145 mutants are severely affected in their development because of mtDNA instability. The
146 mutation is epistatic to *recG1,* indicating that RADA has a more prominent role in plant
147 mitochondrial recombination than it has in bacteria. Furthermore, we found that mtDNA
148 instability triggered by the deficiency of RADA activates genes involved in the suppression of
149 cell cycle progression, partially explaining the growth defect of *radA* plants.
150
151
152 **RESULTS**
153
154 **All plant genomes contain a gene coding for RADA, and RADA from Arabidopsis is**
155 **targeted to both mitochondria and chloroplasts**
156 The Arabidopsis (*Arabidopsis thaliana*) genome was screened for orthologs of RadA
157 and the At5g50340 gene was identified as coding for a protein remarkably similar to bacterial
158 RadA/Sms (45 % similarity), which we named *RADA*. Phylogenetic analysis showed that
159 *RADA* genes are present in all groups of the green lineage, including land plants, green and
160 red algae, as well as in brown algae, diatoms and also in several organisms of the
161 Stramenopile group that are not photosynthetic, such as the water mold *Phytophtora*
162 *infestans* (Supplemental Figure 1). But no RADA ortholog was found in animals or in yeast.
163 While it is probable that plants inherited *RADA* from the prokaryote ancestor of mitochondria
164 or chloroplasts, the high conservation of the sequences did not allow us to infer whether the
165 ancestor was a proteobacterial or a cyanobacterial RadA. Sequence alignments
166 (Supplemental Figure 2) showed that plant RADA have all the important functional motifs that
167 have been described for bacterial RadA/Sms (Cooper et Lovett, 2016; Marie et al., 2017). In
168 addition, plant RADA sequences have non-conserved N-terminal extensions predicted to be
169 organellar targeting peptides. This was tested by expression of N-terminal fusions to GFP.
170 Fusion proteins were constitutively expressed in transgenic Arabidopsis plants under a
171 strong constitutive promoter and found targeted to both chloroplasts and mitochondria, as
172 shown by co-localization with the autofluorescence of chlorophyll and the red fluorescence of
173 MitoTracker® (Figure 1A-C). The N-terminal part of RADA was sufficient to drive targeting to

174 both organelles (Figure 1B), but the full-length fusion localized in chloroplasts mainly in
175 discrete speckles that could be nucleoids, according to co-localization with PEND:dsRED
176 used as nucleoid marker (Figure 1A and D). A previous report described that, in rice, RADA
177 is targeted to the nucleus (Ishibashi et al., 2006). This was inferred from immunodetection
178 with an antibody raised against the recombinant protein. However, our results did not show
179 any hint that RADA could also be a nuclear protein. Thus, RADA is apparently a dually
180 targeted organellar protein, like RECG1 and several other factors involved in the
181 maintenance of organellar genomes (Gualberto et Newton, 2017).
182 Expression data available at Genevestigator (https://genevestigator.com) indicate that
183 *RADA* is preferentially expressed in hypocotyls and in the shoot apex (Supplemental
184 Figure 3A). In line with these data expression of a promoter:GUS fusion construct was found
185 increased in young shoots, in sepals and in the stigma (Supplemental Figure 3B).
186
187 **Structural and functional conservation of plant RADA as compared to bacterial RadA**
188 A three dimensional model of Arabidopsis RADA was built (Figure 2B), based on the
189 known structure of *Streptococcus pneumoniae RadA* (Marie et al., 2017). The RadA
190 structure comprises an N-terminal C4 zinc-finger, required for the interaction with RecA, and
191 two main domains: a RecA-like ATPase domain and a Lon protease-like domain. The RecA-
192 like ATPase domain comprises the Walker A and B motifs, and a RadA-specific KNRFG
193 sequence (Supplemental Figure 2 and Figure 2A). The Walker A and KNRFG motifs are
194 indispensable for the branch migration function of the protein, and are also involved in the
195 DNA-binding and helicase activities of RadA (Cooper et Lovett, 2016; Marie et al., 2017). In
196 bacteria, Walker A and KNRFG mutants are dominant negative, interfering with the function
197 of the wild-type protein. The structural similarity between RadA and RecA suggests
198 functional similarities, but while RecA specialized in the recognition of homologous
199 sequences and strand invasion, RadA rather evolved for driving branch migration. Finally,
200 the C-terminal P-domain of RadA is similar to the Lon protease-like domain of RecA, but it is
201 an inactive domain, since the residues involved in protease activity are not conserved, and
202 no protease activity could be detected (Inoue et al., 2017). Rather, this domain is involved in
203 the binding to DNA and it works as a scaffold for the protein architecture, promoting its
204 oligomerization as hexameric rings (Inoue et al., 2017; Marie et al., 2017).
205 We have tested the ability of plant RADA to complement *Escherichia coli* RadA in the
206 repair of genotoxic stress-induced DNA lesions. A *radA785(del)::kan* strain was used for
207 complementation assays, and Arabidopsis RADA and *E. coli* RadA were expressed from the
208 low-copy number plasmid pACYC. As described by others, we found that the *radA* strain was
209 little affected by genotoxic treatments as compared to WT (Beam et al., 2002; Cooper et al.,
210 2015). The conditions we found best to test complementation were in the presence of

211 ciprofloxacin, an inhibitor of gyrase that induces DNA DSBs. In a spot assay, the growth of
212 radA-deficient cells was much reduced as compared to WT ones. Expression of Arabidopsis
213 RADA could complement the ciprofloxacin-triggered growth defect as well as bacterial RadA
214 cloned in the same expression vector (Figure 2C). Therefore plant RADA can functionally
215 substitute bacterial RadA in the repair of DNA damages induced by ciprofloxacin.
216
217 **RADA is an ssDNA-binding protein that stimulates branch migration in strand-**
218 **exchange reactions**
219 The Arabidopsis cDNA sequence minus the first 48 codons coding for the putative
220 organellar targeting sequence was cloned in bacterial expression vector pET28a, fused to an
221 N-terminal His-tag. A mutant sequence was prepared to express a Walker A-deficient protein
222 (K201A). The mutation of the equivalent position in *E. coli* RadA abolished DNA-dependent
223 ATPase activity and generated a dominant negative *radA* allele (Cooper et al., 2015; Cooper
224 et Lovett, 2016). According to the structure of the protein bound to ADP the mutation should
225 not affect ATP or ADP binding, but ATPase activity is lost (Supplemental Figure 4).
226 Both WT RADA and K201A could be expressed and purified as soluble proteins
227 (Supplemental Figure 5A). By gel filtration the purified WT protein resolved as two peaks of
228 high molecular weight (Supplemental Figure 5B), indicating different degrees of protein
229 oligomerization. Dynamic light scattering analysis of the smaller size oligomer showed that it
230 was mainly constituted by a monodispersed particle of about 340 kDa, consistent with a
231 hexameric RADA complex (Supplemental Figure 5C). EMSA experiments showed that both
232 peak fractions could bind to an ssDNA oligonucleotide probe and give rise to complexes of
233 same apparent size (Supplemental Figure 5D).
234 The purified proteins were tested in EMSA experiments with different DNA structures
235 as substrates, including ssDNA, dsDNA, fork-like structures and double-stranded molecules
236 containing 5' or 3' ssDNA overhangs. Using the same probe concentrations and increasing
237 concentrations of recombinant protein we found that RADA could bind to all structures
238 containing ssDNA regions. It could also bind dsDNA, but with much less affinity (Figure 3A).
239 In our experiments we found that higher molecular weight complexes could be formed.
240 These could not be well resolved in standard gel migration conditions, but in 4.5 %
241 polyacrylamide gels and at lower voltage we could resolve these complexes formed with
242 ssDNA, and found that they were promoted by the presence of ATP or ADP (Figure 3B).
243 Such higher molecular weight complexes could correspond to the polymerization of RADA on
244 ssDNA, forming nucleofilaments. We did not see significant differences in binding with the
245 K201A mutant protein, which seemed to bind ssDNA with equivalent affinity as the WT
246 protein. The sequence specificity of RADA binding to ssDNA was tested in competition
247 experiments. In these experiments poly-dT, poly-dC and poly-dG could compete binding as

248 efficiently as the homologous probe that was used, while poly-dA was less efficient as a
249 competitor (Figure 3C). Thus, Arabidopsis RADA binds preferentially to ssDNA, with little
250 sequence specificity.
251 The branch migration activity of plant RADA was also tested, using an *in vitro* strand-
252 exchange reaction promoted by bacterial RecA. RecA, in the presence of ATP and bacterial
253 single-strand binding protein SSB, can initiate the invasion of dsDNA by homologous ssDNA
254 and promote branch migration till the final heteroduplex product is completed. In the
255 presence of plant RADA the branched intermediates were resolved faster, leading to an
256 earlier appearance of the final nicked double-stranded circular product (Figure 4A). The
257 faster resolution of recombination intermediates was reproducibly observed in six
258 independent experiments (Figure 4B).
259 To test whether RADA-promoted branch migration requires interaction with RecA,
260 assays were arrested by freezing at a time point (7 min) when there was already
261 accumulation of branched intermediates, but no visible final heteroduplex product (Figure 4C
262 left panel). The reaction mix was deproteinated and the purified nucleic acids added to new
263 reaction mixes, in the presence or absence of RADA. In the absence of both RecA and
264 RADA the branched intermediates could not spontaneously evolve and remained stable
265 (Figure 4C middle panel), but in the presence of RADA they were converted to the final
266 product, showing that plant RADA alone can promote branch migration (Figure 4C right
267 panel). This departs from what was described for bacterial RadA, whose function seems to
268 depend from its interaction with RecA. However, RADA is not a recombinase redundant with
269 RecA, because RADA alone in the absence of RecA is not able to initiate the strand-invasion
270 reaction (Figure 4D). This result diverges from a previous report that claimed that plant
271 RADA is able to promote invasion of dsDNA by homologous ssDNA (Ishibashi et al., 2006).
272 Finally, in the same experimental conditions the K201A mutant protein was unable to
273 promote branch migration, and rather completely inhibited the reaction (Figure 4E). That
274 could be because the incapacity of the mutant protein to migrate along the heteroduplexes
275 blocks the activity of RecA. The result is consistent with the dominant negative effect of the
276 equivalent mutation in *E. coli* RadA (Cooper et al., 2015).
277
278 **Arabidopsis plants deficient in RADA are severely affected in their development and**
279 **fertility**
280 We could retrieve several potential *radA* loss-of-function (KO) lines from available
281 Arabidopsis T-DNA insertion collections, from which two (*radA-1* and *radA-2*) could be
282 validated, both in the Col-0 background, with T-DNA insertions in exons 8 and 5 respectively
283 (Figure 5A). Homozygous plants from both mutant lines displayed severe phenotypes of
284 retarded growth of both leaves and roots, and of distorted leaves showing chlorotic sectors

285 (Figure 5B-D). The phenotype was fully penetrant, with all homozygous mutants displaying
286 the phenotype. Transmission electron microscopy (TEM) showed that *radA* mesophyll cells
287 were almost indistinguishable from WT, with chloroplasts that were morphologically normal.
288 On the other hand, mitochondria looked enlarged in size, and less electron dense as
289 compared to those from WT leaves (Supplemental Figure 6). This suggested that it is the
290 mitochondrion that is predominantly affected in *radA*. The severe dwarf phenotype could be
291 partially relieved by growing *radA* plants under a short day photoperiod (8h light/16h dark). In
292 such conditions plants revealed extended juvenility, with dramatic elongation of lifespan and
293 development of aerial rosettes (Figure 5E). A similar phenotype of perennial growth under
294 short days was described for Arabidopsis *msh1* mutants, deficient in the homolog of bacterial
295 mismatch repair protein MutS and affected in mtDNA stability (Xu et al., 2012).
296 To fully confirm that these phenotypes were because of a deficiency in RADA, *radA-1*
297 plants were complemented with the WT *RADA* gene expressed under its own promoter.
298 Heterozygote *radA-1* plants were transformed and homozygous plants that also contained
299 WT *RADA* as a transgene were segregated in the T2 generation. These were phenotypically
300 normal (Figure 5B), confirming the complementation and the linkage of the growth defects to
301 the *radA* allele.
302 Arabidopsis *radA* produces flower stems with very small siliques that mainly contain
303 aborted seeds. The few seeds produced are heterogeneous in shape and few are able to
304 germinate (Figure 6A and 6B). Pollen stained positive by Alexander staining, suggesting that
305 it was viable. That was confirmed by the successful transmission of the *radA* allele in crosses
306 using *radA* pollen. But pollen production was much reduced compared to WT, and many
307 pollen grains were of aberrant size and shape (Figure 6C). Regarding female organs, the
308 stigma displayed elongated and fully differentiated papillae, but with no attached pollen
309 grains (Figure 6D). That could be because papillae cells are modified and unable to bind
310 pollen, or because the stigma develops and is receptive before the pollen matures. To test
311 whether *radA* female gametes are viable emasculated flowers from WT or *radA* were
312 pollinated with WT pollen and ovules were observed before and after pollination. The mature
313 unfertilized *radA* ovules looked morphologically normal and alike WT ovules (Figure 6E).
314 Three days after pollination virtually all WT ovules were fertilized and showed a developing
315 embryo, but only 1/6th of the *radA* ovules had developing embryos (Figure 6E). No
316 elongation of the pollinated pistils was observed even at seven days after pollination
317 (Figure 6F) showing that normal pollen could not fertilize the apparently normal *radA* ovules,
318 potentially because of a deficiency in pollen germination in the stigma of *radA* plants. It is
319 tempting to speculate that it is because of enhanced expression of RADA in the stigmata, as
320 suggested by the promoter:GUS results. Thus, the partial sterility of *radA* would be due to
321 both male and female defects.

322

323 ***radA* mutants are affected in the stability of the mitochondrial genome**

324 Several Arabidopsis mutants affected in recombination functions (ex: *msh1, osb1,*
325 *recA2*, *recA3, recG1*) show, in normal growth conditions, increased ectopic recombination of
326 the mtDNA across intermediate-size repeats (IRs), and the severity of the molecular
327 phenotype normally correlates with the severity of the developmental phenotypes (Arrieta-
328 Montiel et al., 2009; Gualberto et Newton, 2017; Zaegel et al., 2006). The *radA* mutants were
329 thus also tested for such molecular phenotype. Plants from both *radA-1* and *radA-2* lines of
330 the second homozygous generation were grown *in vitro* and four were selected according to
331 the severity of growth defect phenotype (Figure 7A). The relative copy number of the
332 different mtDNA regions in these plants was quantified by qPCR, using a set of primer pairs
333 spaced about 5 kb apart across the genome, as described (Wallet et al., 2015). Dramatic
334 changes in the stoichiometry of mtDNA sequences were observed in all plants (Figure 7B).
335 These affected similar regions of the genome in the individual plants, but the amplitude of the
336 changes was higher in the severely affected plants (*radA-1#1* and *radA-2#1*) than in the
337 mildly affected ones (*radA-1#2* and *radA-2#2*). An increase in copy number of large genomic
338 regions could be observed, that could be as high as seven fold. Several of the observed
339 events of stoichiometry variation corresponded to regions flanked by pairs of directly oriented
340 repeats, including the pair of repeats A (556 bp), F (350 bp), L (249 bp), and EE (127 bp)
341 (Figure 7B). This suggested that the process at play was the same as that described for
342 repeat EE in the *RECG1* KO mutant, *i.e.* the looping out of a circular subgenome by
343 recombination across directly oriented IRs, followed by its autonomous replication (Wallet et
344 al., 2015). We tested by qPCR the accumulation of crossover products for repeats F, L and
345 EE, as previously described (Miller-Messmer et al., 2012; Wallet et al., 2015). As expected,
346 in all plants a significant increase in crossover products *versus* WT levels was observed for
347 all analyzed repeats (Figure 7C), with a significantly higher accumulation in the more affected
348 plants than in the mildly affected ones. Recombination resulted in the asymmetrical
349 accumulation of mainly one of the two crossover products, with the remarkable exception of
350 recombination involving the pair of repeats L, which resulted in the accumulation of only one
351 of the reciprocal crossover products in mildly affected plants, while both products
352 accumulated in the severely affected plants. As described before, asymmetric recombination
353 could be because of repair by the break-induced replication (BIR) pathway (Christensen,
354 2018; Gualberto et Newton, 2017). Big differences in the relative accumulation of
355 recombination products were seen, depending on the pair of repeats analyzed. But these
356 values are misleading, because compared to the basal levels that exist in WT plants. Thus, a
357 30 fold increase in recombination product L-1/2 might be equivalent to a 1000 fold increase
358 in product EE-2/1, because the former is already quite abundant in WT Col-0 and easily

359 detected by hybridization, while the latter is virtually absent in WT (Wallet et al., 2015; Zaegel
360 et al., 2006). Analysis of recombination involving repeats A was not possible, because the
361 size of the region to be amplified (larger than 600 bp) is not compatible with qPCR.
362 Because RADA is also targeted to chloroplasts the plastidial DNA (cpDNA) of *radA*
363 plants was likewise scanned for changes in sequence stoichiometry by qPCR. No changes
364 were detected between mutant and WT, apart from a slight general increase in cpDNA copy
365 number in several individual plants, but below two-fold and probably not significant. We
366 confirmed this result by Illumina DNAseq of four individual *radA-1* plants. The normalized
367 coverage of the cpDNA did not reveal any changes in sequences stoichiometry as compared
368 to WT plants (Figure 8A). No major proportion of indels was detected neither. We also
369 checked whether *radA* plants could have increased rearrangements of the cpDNA, as
370 described for Arabidopsis *why1why3* and *why1why3reca1* Arabidopsis mutants, and for
371 maize *cptK1* (Duan et al., 2020; Le Ret et al., 2018; Zampini et al., 2015). Analysis by PCR
372 using divergent primers has been used before to detect increased rearrangements of the
373 cpDNA (Duan et al., 2020; Marechal et al., 2009). But in our hands, after testing six pairs of
374 primers described in the literature we just obtained either negative or irreproducible results.
375 We have therefore developed a pipeline for identification of Illumina reads corresponding to
376 cpDNA rearrangements (Supplemental Figure 7). The *radA* sequence libraries contained a
377 slightly higher proportion of rearrangements as compared to WT, but the factor was below
378 two-fold (Figure 8B), *i.e.* too low to be considered as responsible for the severe growth defect
379 of *radA* plants. Thus, in contrast to the major effects observed on mtDNA maintenance, the
380 loss of RADA apparently does not significantly affect the stability of the cpDNA in
381 Arabidopsis.
382 In order to dissociate mitochondrial effects of *radA* from possible effects on the
383 chloroplast we tried to hemicomplement the *radA* mutant with a construction corresponding
384 to RADA fused to either a specific mitochondrial targeting sequence (AOX1:RADA) or to a
385 plastid targeting sequence (RBCS:RADA), under control of the *RADA* promoter (Figure 9A).
386 These targeting sequences had been shown to be sufficient for specific and efficient
387 organellar targeting (Carrie et al., 2009). Such constructions were used to transform
388 heterozygote *radA-1* plants, and homozygote plants were selected (AOX1:RADA and
389 RBCS:RADA, respectively, Figure 9B). None of the constructions could achieve complete
390 complementation of the growth defect phenotype. We could not compare the transgenes
391 expression levels, as the transgene-deriving proteins could not be detected with HA-specific
392 antibodies on total plant extracts, from either leaves or inflorescences. Nevertheless,
393 AOX1:RADA plants displayed less severely reduced growth than RBCS:RADA plants
394 (Figure 9B), and not the deformed leaves phenotype characteristic of non-complemented
395 *radA-1* homozygote mutants segregated at the T2 generation from heterozygote plants.

396 Analysis of the accumulation of cross-over product L-1/2 also revealed decreased
397 accumulation in AOX1:RADA as compared to *radA-1* or RBCS:RADA plants (Figure 9C).
398 Taken together, the data from hemicomplemented plants also suggests that the severe
399 growth phenotype of *radA* is mainly because of the effects on mitochondrial genome stability,
400 and not because of chloroplast dysfunction and indirect effects on mitochondria. But
401 RBCS:RADA plants also seemed slightly less affected than the non-complemented mutant
402 (Figure 9B), implying that there is also a plastidial component in the growth defect phenotype
403 of *radA*.
404
405 **The *radA* mutation is synergistic with *recA3* but not with *recG1***
406 In bacteria the *radA* mutation is highly synergistic with *recG*. We therefore tested the
407 epistatic relation between Arabidopsis *RADA* and *RECG1,* in *recG1 radA* double mutants. To
408 compare all mutant plants at the first homozygous generation, heterozygous *recG1-2* plants
409 [KO for *RECG1*, (Wallet et al., 2015)] were crossed with *radA-1* heterozygous plants used as
410 pollen donor. In the segregating F2 generation we obtained WT, *recG1-2, radA-1* and
411 *recG1-2 radA-1* double homozygous mutants. In this cross, plants inherit the organellar
412 genomes of accession Ws, which is the genetic background of *recG1-2.* As described, the
413 *recG1-2* single mutants were similar to WT (Wallet et al., 2015). The *radA-1* single mutants
414 developed the same growth defects observed in the Col-0 background. But surprisingly the
415 *recG1-2 radA-1* double mutants were as severely affected in growth as *radA-1* plants, with
416 no evidence of a negative epistasis between the two mutations (Figure 10A). The double
417 mutants were tested for their cumulative effects on mtDNA stability. In the genetic
418 background of the Ws mtDNA the effect of the *recG1* KO mutation was mainly the
419 accumulation of the episome resulting from the recombination across repeats EE (Wallet et
420 al., 2015). We tested the accumulation of this episome in *recG1-2,* in *radA-1* and in the
421 *recG1-2 radA-1* double mutant (Figure 10B). In the first homozygous mutant generation we
422 found mild and equivalent effects of both *recG1-2* and *radA*-1 on the accumulation of the EE
423 episome, 3 fold and 3.3 fold more abundant than the flanking mtDNA regions, respectively.
424 However, in *recG1-2 radA-1* there was a significant increase in copy number of the EE
425 episome, with roughly a 10 fold higher copy number than the flanking regions. Thus, at the
426 molecular level the *recG1-2 radA-1* double mutation has an additive impact on the correct
427 segregation of mtDNA sequences. But contrarily to what was observed in bacteria, in plants
428 the *recG1 radA* double mutants are not more severely affected in growth than *radA* plants,
429 implying that RADA contributes to a higher extent to mitochondrial genome maintenance
430 than RECG1.
431 It was previously shown that *recG1* is synergistic with mutants deficient for *RECA3*
432 (Wallet et al., 2015)*,* which encodes a mitochondrial RecA ortholog that is dispensable,

433 contrarily to RECA2 (Miller-Messmer et al., 2012). Therefore we also tested the epistatic
434 relationship between *radA* and *recA3.* Heterozygous *recA3-2* and *radA-1* mutants (both in
435 Col-0 background) were crossed, but no double homozygous mutants could be retrieved
436 from F2 plants growing on soil. Seeds from sesquimutant *recA3-/- radA+/-* were germinated
437 *in vitro* and seedlings were genotyped, revealing that *recA3 radA* double homozygous
438 mutants can germinate (Figure 10C), but are unable to grow roots and to expand their
439 cotyledons. The seedling lethal phenotype was similar to the one observed for *recA2* (Miller-
440 Messmer et al., 2012), and also for certain later generation *radA* plants, as shown in
441 Figure 7A. Molecular analysis showed that mtDNA stability was greatly affected. While
442 segregating *recA3* single mutant plants showed just mild effects, an overall reduction in copy
443 number as compared to WT seedlings of the same size was observed for the mtDNA of
444 *recA3 radA*, some regions being more than 20 fold reduced or increased as compared to
445 neighboring sequences (Figure 10D). The profiles were equivalent to the one obtained for
446 *recA2* plants, both *recA2* and *recA3 radA* showing dramatic reduction of the regions between
447 repeats L-2 and A-2 and between Large repeat 1-2 and repeat L-1. These sequences are
448 duplicated in the nuclear genome of Col-0 (Stupar et al., 2001) and most probably the
449 reduction corresponds to a complete loss from the mtDNA. A small sequence (278 bp)
450 downstream LR1-2 is unique to the mtDNA, and that sequence is virtually absent in both
451 *recA2* and *recA3 radA.* In contrast, the copy number of the cpDNA was little affected, apart
452 for one of the *recA3 radA* replicates in which a small decrease of about 0.7-fold was
453 observed (Figure 10E). Thus, the seedling lethality can be explained by massive problems in
454 the replication and segregation of the mtDNA. The synergistic effect of the *radA* and *recA3*
455 mutations suggests that the two factors intervene in alternative pathways, and that
456 compromising both of them leads to a defect equivalent to the loss of the main
457 RECA2 dependent recombination pathways.
458
459 **Effects of mtDNA instability on the mitochondrial transcriptome**
460 As discussed above, the instability of the mtDNA in *radA* plants correlated with the
461 severity of the growth defect phenotypes. But in no case we found a significant reduction in
462 copy number of an mtDNA gene, linking the phenotype to a defect in mtDNA gene
463 expression. In order to understand the reason for the *radA* growth defects the relative
464 abundance of most mitochondrial gene transcripts and rRNAs was quantified by RT-qPCR.
465 Surprisingly, no apparent defect in mtDNA gene expression was found. Rather, for most
466 transcripts an increased accumulation was observed, as compared to WT plants of the same
467 size (Figure 11A), up to 8-fold in the case of the *rps4* transcript. Because reshuffling of the
468 mtDNA sequences by recombination can change the expression of non-coding ORFs and/or
469 lead to the expression of chimeric genes we also tested the expression of a few mtDNA

470 ORFs whose transcription could be affected by recombination across IRs. These included
471 *orf195*, a chimera containing the sequence encoding the N-terminus of RPS3 as a result of
472 recombination across repeats A (Figure 11B), *orf315*, which contains the sequence encoding
473 the N-terminus of ATP9 following recombination across repeats G, as well as *orf262a* and
474 *orf255*, which might be transcriptionally activated by recombination involving repeats E, L or
475 H. An 8-fold increase in the abundance of *orf195* and *orf315* transcripts was observed,
476 whose expression is driven by the *rps3* and *atp9* promoters, respectively. Thus, one of the
477 possible reasons for the *radA* growth defects could be the expression of toxic ORFs
478 generated by recombination that could interfere with the assembly or activity of OXPHOS
479 complexes. However, analysis of the later on Blue-Native gels failed to detect any major
480 problem (Figure 11C). Activity staining of Complex I and immunodectection of Complex III
481 also revealed complexes of the same size and abundance as in WT mitochondria.
482
483 **Instability of the mtDNA in *radA* mutants affects cell cycle progression**
484 Scanning electron microscopy (SEM) showed that *radA* epidermal leaf cells were
485 much enlarged as compared to cells of WT leaves, suggesting an inhibition of cell division
486 (Figure 12A). The *radA* leaves also had significantly fewer stomata (384.mm^{-2} in *radA-1*
487 *versus* 779.mm^{-2} in WT, χ^2 test=8.5E-14). To test such a possibility, the nuclear DNA ploidy
488 levels were measured by flow cytometry, in the fully developed first true leaves of 20-day-old
489 *radA* and WT plants (Figure 12B and C). The *radA* leaves displayed a higher proportion of
490 4C and 8C nuclei than WT leaves, and an important reduction in 16C nuclei, suggesting that
491 endoreduplication is inhibited in *radA*. In all *radA* samples an accumulation of intermediate
492 peaks (ex. 8-16C) was observed, but not in WT, also suggesting a blockage of cell cycle
493 progression in S phase, or an induction of programmed cell death. To further explore
494 whether mtDNA instability in *radA* impacts cell cycle progression we quantified nuclear DNA
495 replication in root tips, using the thymidine analog 5-ethynyl-2'-deoxyuridine (EdU). In *radA*
496 the ratio of EdU-positive nuclei was significantly reduced (Figure 12D). Counting of mitotic
497 events in root tips also showed much reduced numbers of cells undergoing mitosis in *radA*
498 (Figure 12E).
499 It is known that cell cycle checkpoints adjust cellular proliferation to changing growth
500 conditions, arresting it by inhibiting the main cell cycle controllers that include cyclin-
501 dependent kinases (CDKs) (Nowack et al., 2012). In plants, *SMR* genes encode inhibitors of
502 CDK-cyclin complexes that are transcriptionally induced in response to changing conditions,
503 integrating environmental and metabolic signals with cell cycle control (Dubois et al., 2018;
504 Hudik et al., 2014; Yi et al., 2014). Interestingly, chloroplastic defects have been shown to
505 induce cell cycle arrest through the induction of *SMR5* and *SMR7* (Duan et al., 2020; Hudik
506 et al., 2014). How these genes are activated remains to be fully elucidated, but the

507 mechanism could involve the activation of the DNA damage response (DDR). This signaling
508 cascade is controlled by the ATM and ATR kinases (Abraham, 2001) that phosphorylate the
509 SOG1 transcription factor, leading to the up-regulation of thousands of target genes,
510 including *SMR5* and *SMR7* (Yoshiyama, 2016; Yoshiyama et al., 2013). We have therefore
511 tested the expression of several cell cycle markers and of several genes that are
512 transcriptionally activated as part of the DDR. These included 14 *SMR* genes, selected cell
513 cycle-related genes and the NAC-type transcription factors ANAC044 and ANAC085 that
514 inhibit cell cycle progression in response to DNA damage through their activation by SOG1,
515 but also in response to heat stress through a SOG1-independent pathway (Takahashi et al.,
516 2019). Among the 14 SMR genes tested we found strong induction of *SMR5* in *radA*
517 (Figure 12F, left panel). But transcription of *SMR7*, whose activation has been described as
518 associated with that of *SMR5* in the case of chloroplastic defects (Hudik et al., 2014; Yi et al.,
519 2014), remained unchanged. ANAC085 was strongly activated in *radA,* more than 30-fold as
520 compared to WT, as well as ANAC044 but to a much lower degree (Figure 12F, right panel).
521 We also observed a low-level induction of the DDR genes *BRCA1* and *RAD51*, and of the
522 *CYCB1;1* gene encoding a cyclin associated with G2 arrest and DSB repair (Weimer et al.,
523 2016).
524 SMR5 is a cyclin-dependent kinase inhibitor that is induced by different conditions
525 leading to oxidative stress (Peres et al., 2007). ROS-dependent transcriptional activation of
526 *SMR5* and of *SMR7* was confirmed in several ROS-inducing conditions (Yi et al., 2014). We
527 have therefore tested whether the induction of *SMR5* in *radA* mutants could be due to the
528 accumulation of ROS. Whole rosettes of WT and *radA* plants of same size were stained with
529 nitro blue tetrazolium (NBT) to reveal O^{2-}, and a much higher accumulation of ROS was
530 indeed confirmed in *radA* plants (Figure 12G). To confirm the effect of ROS on the activation
531 of cell cycle regulators, *radA* and WT plants were grown in the presence of the ROS
532 quencher ascorbic acid, and the expression of selected genes tested. In both WT and mutant
533 seedlings the expression of *SMR5*, *ANAC044*, *ANAC085* and *CDKB1;2* were significantly
534 reduced, as compared to plants grown in the absence of ascorbate, up to 8-fold in the case
535 of *SMR5* in *radA* (Figure 12H). Thus, a component of the *radA* growth phenotype is
536 apparently a retrograde response that activates cell cycle regulators to inhibit cell
537 proliferation. This could be because of the release of ROS as a consequence of mtDNA
538 instability.
539

540 **DISCUSSION**

541

542 The role of RadA (or Sms) in bacterial HR has been described only very recently
543 (Cooper et Lovett, 2016; Marie et al., 2017). RadA is a hexameric helicase loaded by RecA
544 on either side of the D-loop, to allow hybridization of the invading ssDNA with the recipient
545 DNA (Marie et al., 2017). Our results show that plant RADA apparently has similar activity in
546 organelles, but a more essential role in genome maintenance than its bacterial counterpart. A
547 previous report proposed that plant RADA is a nuclear protein (Ishibashi et al., 2006), but our
548 results just showed RADA targeted to mitochondria and chloroplasts, where it probably
549 localizes in nucleoids. That is consistent with the presence of predicted targeting sequences
550 in all plant sequences.

551 The modeled structure of plant RADA suggested that bacterial and plant proteins
552 have similar activities. We established this conservation of activity by showing that
553 Arabidopsis RADA complements the survival of a bacterial *radA* mutant under genotoxic
554 conditions, as efficiently as the *E. coli* protein when brought in *trans*. Similarly, we showed
555 that plant RADA preferentially binds ssDNA and accelerates the *in vitro* strand-exchange
556 reaction initiated by RecA, as described for bacterial RadA (Cooper et Lovett, 2016). As
557 reported for bacterial RadA we found that Arabidopsis RADA is not able to initiate strand
558 invasion, and can only promote branch-migration. However, it was previously reported that
559 the rice ortholog is able to promote D-loop formation (Ishibashi et al., 2006). In that report a
560 different assay system was used, based on the invasion of double-stranded supercoiled
561 plasmid by a labeled oligonucleotide, and the efficiency seemed very low. With the
562 Arabidopsis recombinant protein and in our test system we could not reproduce such an
563 activity.

564 Several differences were observed, between the activities of Arabidopsis RADA and
565 those of bacterial RadA. RADA could bind ssDNA-containing molecules without the need for
566 ADP or ATP. But in the presence of ADP or ATP it formed higher molecular weight
567 complexes with ssDNA, suggesting a higher degree of protein oligomerization. The presence
568 of ATP activates the translocation of bacterial RadA and causes the dissociation of the
569 protein from DNA (Marie et al., 2017). Only the mutant of the ATPase domain remains
570 associated with DNA in the presence of ATP, because it is unable to activate translocation
571 (Marie et al., 2017). In contrast, both the WT Arabidopsis RADA and the Walker A K201A
572 mutant could bind to ssDNA and form high molecular weight complexes in the presence of
573 ATP or ADP. A possible explanation could be that under our test conditions the ATPase
574 activity of RADA is not functional, preventing translocation on the DNA. But that seems
575 unlikely given that the recombinant protein could accelerate *in vitro* strand exchange, and
576 should therefore have translocase activity. Thus, the conditions of interaction of RadA (or

577 RADA) with DNA remain controversial. Marie et al. (2017) observed the binding of bacterial
578 RadA to DNA in the absence of ATP, and translocation in the presence of ATP. Cooper and
579 Lovett (2016) observed RadA binding to DNA only in the presence of ADP, while we
580 observed binding of plant RADA to DNA regardless of the presence of ADP or ATP.
581 Departing also from what was described for bacterial RadA we found that plant RADA by
582 itself can promote branch migration of recombination intermediates, in the absence of RecA,
583 while the interaction with RecA was described as necessary for bacterial RadA activity

584 In bacteria, the mutation of a single branch migration factor is only slightly deleterious
585 for cell growth and DNA repair, and that is particularly true for RadA (Beam et al., 2002;
586 Cooper et al., 2015). In plants however, the single loss of RADA severely affects plant
587 development and fertility. This result also contrasts with the lack of a notable developmental
588 phenotype observed for the Arabidopsis *recG1* mutants (Wallet et al., 2015). It therefore
589 seems that, in plants, RADA has a more important role than RECG1. Since the RuvAB
590 migration pathway is absent in plants, it is possible that HR in plant organelles has evolved
591 by favoring the RADA pathway. Surprisingly, the double mutant *radA recG1* is not more
592 affected in its development than the *radA* single mutant, while in bacteria the mutation of the
593 different branch migration pathways is particularly synergistic (Beam et al., 2002; Cooper et
594 al., 2015). The bacterial *radA recG* double mutant is more severely affected than the *recA*
595 single mutant, indicating that the accumulation of unprocessed branched intermediates is
596 more detrimental to the cell than the lack of recombination. In agreement with this
597 hypothesis, the bacterial triple mutant *recA radA recG* is less affected than the *radA recG*
598 double mutant. In plants, the *recA2* mutant is lethal at the seedling stage, and a double
599 mutant *recA2 recA3* could not be segregated, suggesting a more vital role of recombination
600 in organelles than in bacteria (Miller-Messmer et al., 2012). It is therefore surprising that the
601 mutation of all known branch migration pathways in plants is not more deleterious than the
602 mutation of the recombinase.

603 It is possible that non-processing of recombination intermediates is not as detrimental
604 in plant organelles as in bacteria. But it can also be hypothesized that a further alternative
605 pathway for the processing of recombination intermediates exists in plant organelles. The
606 synergy of the *radA* and *recA3* mutations recalls that observed in the double mutants of
607 bacterial branch migration factors (Cooper et al., 2015). Thus, it might be that RECA3 can
608 process the recombination intermediates created by the RECA2 recombinase, thanks to its
609 branch-migration activity that is intrinsic to RecA-like proteins (Cox, 2007). Furthermore,
610 RECA3 is characterized by the absence of an acidic C-terminal sequence that is found in all
611 other RecA-like proteins, including RECA1 and RECA2 (Miller-Messmer et al., 2012; Shedge
612 et al., 2007). In bacteria, the C-terminus is a site for interaction with many other proteins that
613 regulate RecA activity and its deletion results in a conformational change in the RecA-DNA

614 filament that enhances almost every one of the RecA functions (Cox, 2007). In eukaryotes,
615 RAD51 paralogs can also be involved in the regulation of recombinase functions (Chun et al.,
616 2013; Qing et al., 2011). As an example, XRCC3, which is part of the CX3 complex, is
617 necessary for the stabilization of heteroduplexes and controls the extent of gene conversion,
618 thus fulfilling roles reminiscent of branch migration factors (Brenneman et al., 2002). In this
619 respect, RECA3 might have evolved to display enhanced branch migration activity and to be
620 partially redundant to RADA. Nonetheless, unlike RADA, RECA3 apparently retained strand
621 invasion activity, and could partially complement the bacterial *recA* mutant in the repair of
622 UV-induced lesions (Miller-Messmer et al., 2012). RECA3 is therefore also partially
623 redundant with RECA2. Whereas RECA2 and RADA would have specialized in homologous
624 sequence recognition and invasion and branch migration, respectively, RECA3 would have
625 retained both functions.

626 It is also conceivable that RECA3 acts in an alternative recombination pathway
627 independent of RECA2 and RADA. In the absence of RADA, processing of the intermediates
628 produced by the RECA2 pathway would require activation of the alternative RECA3-
629 dependent recombination pathway. The loss of both RADA and RECA3 would overload the
630 system with unresolved recombination intermediates, which would be lethal for the plant. The
631 accumulation of toxic unresolved structures could be also the cause for the sever growth
632 inhibition observed in later generations of *radA*, as described for Figure 7A. The most
633 affected ones showed similar seedling lethality and root growth inhibition as observed for
634 *recA2* and *recA3 radA.*

635 We show here that the absence of RADA results in a significant increase in mtDNA
636 ectopic recombination. This could be because of the repair of DSBs by error-prone break-
637 induced replication (BIR), triggered by a deficiency in HR functions required for accurate
638 replication-coupled repair (Christensen, 2018; Gualberto et Newton, 2017). It apparently
639 leads to the formation of sub-genomes that replicate more rapidly and without coordination
640 with the rest of the mtDNA, as it was observed in *recG1* for the episome resulting from
641 recombination involving repeats EE (Wallet et al., 2015). The more the structure of the
642 mtDNA is modified, the more the development of the plant is affected. However, no region of
643 the mtDNA containing functional genes is lost, and all mitochondrial genes that were tested
644 are expressed. The expression of tRNAs has not been tested, but no region comprising a
645 tRNA gene is lost in *radA* plants. Thus, we could not correlate the developmental phenotypes
646 with the reduced expression of a transcript for an OXPHOS subunit, or for a factor required
647 for OXPHOS subunit synthesis and complex assembly. The BN gel analysis also did not
648 reveal any obvious defect in OXPHOS complexes. Nevertheless, the increase in ectopic
649 recombination can lead to the creation and expression of chimeric genes that could encode
650 toxic proteins (Hanson et Bentolila, 2004; Touzet et Meyer, 2014).

651 Despite dual targeting, the absence of RADA does not seem to have deleterious
652 effects in the chloroplast. Analysis of Illumina sequences revealed only a slight increase in
653 reads corresponding to cpDNA rearrangements, which can hardly be correlated with the
654 severe growth defects of *radA* plants. As discussed elsewhere, that might be because of the
655 absence of IRs in the cpDNA of Arabidopsis that can promote genome instability in
656 conditions of replicative stress (Gualberto et Newton, 2017). Mutants of *RECG1* and *RECA2*
657 that are also dually targeted did not reveal either any problems in cpDNA maintenance. To
658 dissociate the effects of RADA in mitochondria and plastids we performed
659 hemicomplementation of the Arabidopsis *radA* mutant with the AOX1:RADA or RBCS:RADA
660 constructs, whose products were expected to be specifically targeted to either mitochondria
661 or plastids, respectively. Full complementation of the growth defect phenotype was not
662 achieved, but mutant plants complemented with the AOX1:RADA construct were less
663 affected in their growth than those complemented with RBCS:RADA. Taken together, the
664 TEM images, the mtDNA and cpDNA genomic analyses and the hemicomplementation
665 results all agree that RADA is particularly important in the mitochondrial compartment.
666 The severe developmental phenotypes elicited in *radA* mutants seem to partially
667 result from a mitochondrial retrograde signaling that promotes inhibition of cell cycle
668 progression. The cell cycle is an energy demanding process that can be arrested by defects
669 in respiration or photosynthesis (Riou-Khamlichi et al., 2000). Several studies have shown
670 that chloroplastic defects lead to altered cell cycle regulation including reduced cell
671 proliferation and premature endoreduplication (Duan et al., 2020; Hudik et al., 2014;
672 Pedroza-Garcia et al., 2019). That seems to be also the case in *radA,* as suggested by the
673 increased size of epidermal cells and confirmed by determination of nuclear ploidy, analysis
674 of EdU incorporation and mitotic activity, although in this case endoreduplication was
675 reduced in the *radA* mutant. Our results thus show that defects in the maintenance of
676 mitochondrial genome integrity can also interfere with cell cycle progression in plants.
677 Consistently, expression of *RADA* is higher in proliferating tissues, although it does not seem
678 to be cell cycle regulated according to data generated with synchronized BY-2 cells (Trolet et
679 al., 2019), suggesting that maintenance of mitochondrial genome integrity is crucial in highly
680 dividing cells. A reduced mitotic index has also been observed in *recA3 msh1* double
681 mutants, which develop a sever growth defect phenotype similar to *radA* (Shedge et al.,
682 2007). And in Drosophila it has been established that mitochondrial dysfunction activates
683 retrograde signals, including ROS, to modulate cell cycle progression (Owusu-Ansah et al.,
684 2008)
685 In the case of chloroplast dysfunction, it has been suggested that accumulation of
686 ROS is responsible for the observed cell cycle arrest. Similarly, it is possible that
687 mitochondrial genome instability in *radA* results in sub-optimal function of the OXPHOS

688 complexes and in ROS production, triggering the arrest of the cell cycle and the
689 developmental phenotypes observed. But just functional deficiency of OXPHOS complexes
690 does not *per se* activate regulators of cell cycle, since in mutants of complex I there was no
691 evidence for the activation of genes such as SMR5 or SMR7 (Meyer et al., 2009). In several
692 chloroplast-deficient mutants such as *crl* or the triple *reca1why1why3*, ROS accumulation is
693 thought to activate the DNA Damage Response master regulator SOG1, leading to cell cycle
694 arrest and activation of DNA repair (Duan et al., 2020; Hudik et al., 2014; Pedroza-Garcia et
695 al., 2019). Indeed, DDR mutants and particularly *sog1* are hypersensitive to genotoxins
696 targeting organelles (Pedroza-Garcia et al., 2019) and ROS accumulation leads to SOG1
697 activation through its phosphorylation by the ATM kinase (Yi et al., 2014). However, recent
698 results showed that SOG1, ATM and ATR are not required for the activation of *SMR5* and
699 *SMR7* in the *crl* mutant, in which chloroplast homeostasis is severely compromised (Li et al.,
700 2020), suggesting that alternative pathways exist to control cell cycle progression depending
701 on chloroplast activity. In line with this hypothesis, we found that a number of SOG1 targets
702 are only slightly mis-regulated in *radA* mutants. In addition, treatment with the ROS
703 scavenger ascorbate only partially rescued the activation of genes involved in cell cycle
704 arrest in the mutant. Interestingly, we observed that *ANAC085*, a direct SOG1 target that can
705 also be activated directly by abiotic stress such as heat (Takahashi et al., 2019) is strongly
706 upregulated in the *radA* mutant, and that this induction is largely independent of ROS
707 accumulation. It is thus tempting to speculate that retrograde signaling triggered by
708 mitochondrial genome instability also relies on alternative pathways independent of canonical
709 DDR signaling, and only partly mediated by ROS accumulation (Supplemental Figure 8).
710 Further work will be required to fully decipher how defects in the maintenance of organellar
711 genomes integrity lead to an inhibition of cell cycle progression.
712

713 **METHODS**

714

715 **Plant Material:**

716 Arabidopsis T-DNA insertion mutant lines, all in the Col-0 background, were obtained from
717 the Nottingham Arabidopsis Stock Centre (*radA-1*: SALK_097880, *radA-2*:
718 WiscDsLoxHs058_03D). Plant genotypes were determined by PCR using gene and T-DNA
719 specific primers. Seeds were stratified for 3 days at 4 °C and plants were grown on soil or on
720 half-strength MS medium (Duchefa) supplemented with 1 % (w/v) sucrose, at 22 °C. DNA
721 was extracted using the cetyltrimethylammonium bromide method. RNA was extracted using
722 TRI Reagent (Molecular Research Centre, Inc.). For RT-qPCR experiments, 5 µg of RNA
723 were depleted from contaminating DNA by treatment with RQ1 RNase-free DNase
724 (Promega) and were reverse-transcribed with Superscript IV Reverse Transcriptase (Thermo
725 Fisher Scientific), according to the manufacturer's protocol using random hexamers. For
726 mutant complementation, the WT *RADA* gene and promoter sequence was cloned in binary
727 vector pGWB613, fused to a C-terminal 3xHA tag, and used to transform heterozygous
728 *radA–1* plants. Expression of the transgene in the T1 transformants was monitored by
729 western-blot with a HA-specific antibody. For hemicomplementation, i) the promoter
730 sequence and 5' UTR of *RADA*, ii) the N-terminal sequence (49 codons) of soybean
731 alternative oxidase 1 (AOX1; NM_001249237) or the N-terminal sequence (80 codons) of the
732 small subunit of ribulose bisphosphate carboxylase (RBSC; At1g67090), and iii) the RADA
733 sequence minus its first 86 codons fused to a C-terminal HA epitope and Nos terminator,
734 were assembled together by MultiSite Gateway cloning in vector pB7m34GW,0
735 (https://gatewayvectors.vib.be/), giving constructions AOX1:RADA and RBCS:RADA
736 respectively. These constructs were used to transform heterozygous *radA-1* plants by floral
737 dip. For promoter:GUS fusion expression analysis, the *RADA* promoter and 5'-UTR
738 (1114 bp) was cloned in vector pGWB633 and transformed into Col-0 plants.

739

740 **Isolation of mitochondria and Blue Native PAGE**

741 Arabidopsis mitochondria were prepared from the aerial part of three-week old plants grown
742 on soil, by differential centrifugation and step density gradients as described (Meyer et al.,
743 2009). Arabidopsis mitochondrial complexes were solubilized with 1.5 % dodecylmaltoside
744 and analysed on BN-PAGE 4-13% (w/v gels, as described (Wittig et al., 2006). Blue staining
745 and in gel NADH dehydrogenase activity were as described (Sabar et al., 2005).

746

747 **Bioinformatics analysis**

748 Bacterial and plant sequences were identified in the databases by BLASTP and TBLASTN.
749 Alignments were constructed with T-Coffe implemented in the Macvector package. Targeting

750 prediction were tested using the SUBA web site (http://suba.plantenergy.uwa.edu.au)
751 Phylogenetic trees were built with PhyML v3.1 (www.phylogeny.fr) using the neighbor-joining
752 method implemented in the BioNJ program. Graphical representations were performed with
753 TreeDyn (v198.3). The Arabidopsis RADA structure was modeled on the structure of RadA
754 from *Streptococcus pneumoniae* (pdb: 5LKM), using Modeller
755 (http://salilab.org/modeller/about_modeller.html). For Illumina sequence analysis of the
756 cpDNA, reads were aligned against the Arabidopsis reference genomes using Burrows-
757 Wheeler Aligner (BWA) (Li et Durbin, 2009) and filtered to keep only those mapping to the
758 cpDNA. The coverage was extracted with Bedtool genomecov (Quinlan et Hall, 2010) and
759 coverage positions were rounded down to the upper kb and the coverage of each 1 kb-range
760 was normalized relative to 1,000,000 total Arabidopsis reads. For analysis of rearranged
761 sequences, reads properly pairing to the cpDNA were filtered to only keep those showing a
762 short-clipping sequence (threshold 20 nucleotides) and no indel (looking for the presence of
763 a S in the CIGAR string without any I,D and H). The short-clipping sequences were then
764 extracted with SE-MEI/extractSoftclipped (github.com/dpryan79/SE-MEI) and aligned using
765 bowtie2 (Langmead et Salzberg, 2012) against the cpDNA. The positions of the short-
766 clipping sequences mapping the cpDNA and of their relative read were rounded down to the
767 upper kb to analyse the localization of the rearrangement. Those corresponding to the
768 isomerization that results from the recombination involving the large inverted repeats were
769 filtered out.

770

771 **Intracellular Localization**

772 The cDNA sequence coding the Arabidopsis RADA N-terminal domain (first 174 codons) was
773 cloned into pUCAP-GFP, derived from pCK-GFP3 (Vermel et al., 2002), and the expression
774 cassette under control of a double 35S promoter was transferred to the binary vector pBIN+.
775 For full protein fusion to GFP the gene sequence and 5'-UTR (from -156 to 4172 relative to
776 the start codon) was cloned in vector pUBC-paGFP-Dest (http://n2t.net/addgene:105107).
777 Arabidopsis Col-0 plants were transformed by the floral dip method and leaves of selected
778 transformants were observed on a Zeiss LSM700 confocal microscope. The fluorescence of
779 GFP and chlorophyll was observed at 505 to 540 nm and beyond 650 nm, respectively. For
780 mitochondrial co-localization, leafs were infiltrated with a 1/1000 dilution of MitoTraker®
781 orange (Thermo Fisher Scientific) solution. Excitation was at 555 nm and observation at 560-
782 615 nm. Nucleoid co-localization was tested by biolistic co-transfection in *Nicotiana*
783 *Benthamiana* epidermal leaf cells with a PEND:dsRED construction (Melonek et al., 2012).
784
785

786 **In vitro strand exchange reaction**

787 Recombination assays were performed with single-strand linear ΦX174 virion DNA and
788 double strand circular ΦX174 RFI DNA (New England Biolabs) linearized with PstI in 20 mM
789 Tris-acetate pH 7.4, 12.5 mM phosphocreatine, 10 U/mL creatine kinase, 3 mM ammonium
790 glutamate, 1 mM dithiothreitol, 2 % glycerol and 11 mM magnesium acetate. In our
791 conditions, 20.1 µM (in nucleotides) linear single strand DNA (ssDNA), 6.7 µM RecA (New
792 England Biolabs), 2 µM RADA are incubated with buffer for 8 min at 37 °C. Then, 20.1 µM (in
793 nucleotides) linear double-strand DNA (dsDNA) is added and the whole reaction is incubated
794 for 5 min at 37 °C. Finally, strand exchange is initiated by adding 3 mM ATP and 3.1 µM SSB
795 (Merck). Aliquots are stopped at indicated times by addition of 12 µM EDTA and 0.8 % SDS.
796 Strand exchange products were analyzed on 0.8 % agarose gels run at 4 °C in Tris-acetate
797 EDTA buffer at 50 V and visualized after migration by ethidium bromide staining. For
798 reactions terminated in the absence of RecA, the RecA-initiated strand exchange reaction
799 was stopped at the indicated time and DNA was deproteinized by phenol-chloroform
800 extraction followed by ethanol precipitation. The DNA pellet was solubilized in reaction buffer,
801 2 µM RADA was added and the reaction was further incubated at 37 °C for the indicated
802 time, before quenching with 12 µM EDTA and 0.8 % SDS.

803

804 **DNA Binding Assays**

805 For electrophoretic mobility shift assays (EMSA) the purified recombinant protein (50-
806 500 fmol according to the experience) was incubated with oligonucleotide probes (0.01 pmol-
807 10 fmol) 5'-radiolabeled with [γ-^{32}P]ATP (5000 Ci/mmol; PerkinElmer Life Science). Different
808 dsDNA structures were prepared by annealing the radiolabeled sense oligonucleotides with a
809 twofold excess of unlabeled complementary oligonucleotide and purified on non-denaturing
810 polyacrylamide gels. The binding reactions were performed in 20 mM Tris-HCl pH 7.5,
811 50 mM KCl, 5 mM $MgCl_2$, 0.5 mM EDTA, 10 % glycerol, 1 mM DTT and protease inhibitors
812 (Complete-EDTA; Roche Molecular Biochemicals), incubated at 20 °C for 20 min and run on
813 8 or 4.5 % polyacrylamide gels in Tris-Borate-EDTA buffer at 4 °C. After drying gels were
814 revealed using an Amersham Typhoon phosphorimager (GE Healthcare Life Sciences). For
815 competition assays, labeled probe and unlabeled competitor were added simultaneously to
816 the reaction mixture.

817

818 **Recombinant proteins**

819 Constructs pET28-RADA minus first 48 codons and pET28A-RADA[K201A] were used to
820 express recombinant proteins in *E. coli* Rosetta 2 (DE3) pLysS (Novagen). Transformed
821 bacteria were grown at 37 °C until OD_{600nm} = 0.6. Cultures were then chilled to 4 °C for
822 30 min before addition of 0.5 mM isopropyl b-D-1-thiogalactopyranoside (IPTG) and

823 overnight incubation at 18 °C. After growth cells were pelleted, resuspended in 50 mM Tris-
824 HCl pH 8.0, 5 % glycerol, 300 mM NaCl, 10 mM imidazole, supplemented with 1 mM PMSF
825 and 1 X cOmplete protease inhibitors (Merck) and lysed with a French press under 1200 PSI.
826 The crude lysate was sonicated for 3 min, clarified by 25 min centrifugation at 17700 g and
827 filtrated trough a Filtropur S plus 0.2 µm filter (Sarstedt). The recombinant RADA and
828 RADA[K201A] proteins were affinity purified in a precalibrated HisTrap FF Crude (GE
829 Healthcare Life Sciences) column run at 0.5 mL/min, washed with 50 mM Tris-HCl pH 8.0,
830 300 mM NaCl, 5 % glycerol, 50 mM imidazole and eluted with a 50-500 mM imidazole
831 gradient. The recombinant protein fractions was further purified by gel filtration on Superdex
832 S200 columns and aliquots were flash frozen in liquid nitrogen and stored at -80 °C. RADA
833 concentration was determined by spectrophotometry using an extinction coefficient of
834 42,440 M^{-1} cm^{-1}.
835
836 **Bacterial complementation**
837 The *E. coli* TOP10 strain was used for routine cloning, whereas the BW25113 *radA+* and
838 JW4352 *radA785(del)::kan* were used for complementation assays. The Arabidopsis RADA
839 cDNA (sequence coding for amino acids 137 to 627) or the *E. coli* RadA/Sms sequence were
840 cloned between the PstI and BamHI restriction sites of the pACYCLacZ vector (Miller-
841 Messmer et al., 2012) under the control of the *lac* promoter. Both constructs were introduced
842 in the JW4352 strain. The pACYCLacZ empty vector was introduced in the BW25113 and
843 JW4352 strains as control. Bacteria were grown in LB supplemented with 10 µg/mL
844 chloramphenicol till OD_{600nm} = 0.4 before addition of 2.5 mM IPTG. At OD_{600nm} = 1.2 bacteria
845 were diluted 10^4 fold and grown on LB agar plates supplemented with 15 nM ciprofloxacin,
846 2 mM IPTG and 10 µg/mL chloramphenicol.
847
848 **qPCR Analysis**
849 qPCR experiments were performed in a LightCycler480 (Roche) in a total volume of 6 µL
850 containing 0.5 mM of each specific primer and 3 µl of SYBR Green I Master Mix (Roche
851 Applied Science). The second derivative maximum method was used to determine Cp values
852 and PCR efficiencies were determined using LinRegPCR software (http://LinRegPCR.nl).
853 Three technical replicates were performed for each experiment. Results of qPCR and RT-
854 qPCR analysis were standardized as previously described (Wallet et al., 2015). The recently
855 corrected Arabidopsis Col-0 mtDNA sequence was taken as reference (Sloan et al., 2018).
856 Quantification of mtDNA and cpDNA copy numbers used a set of primer pairs located along
857 the organellar genomes, as described previously (Le Ret et al., 2018; Wallet et al., 2015).
858 Results were normalized against the UBQ10 (At4G05320) and ACT1 (At2G37620) nuclear
859 genes. The accumulation of ectopic recombination in mtDNA was quantified using primers

860 flanking each repeats, as described (Miller-Messmer et al., 2012). The COX2 (AtMG00160)
861 and 18S rRNA (AtMG01390) mitochondrial genes and the 16S rRNA (AtCG00920)
862 chloroplast gene were used for normalization. For RT-qPCR experiments the GAPDH
863 (At1G13440) and ACT2 (At3G18780) transcripts were used as standards.
864
865 **Sequencing**
866 Total leaf DNA of WT and *radA-1* plants was quantified with a QuBit Fluorometer (Life
867 Technologies) and libraries were prepared with the Nextera Flex Library kit, according to
868 manufacturer's recommendations (Illumina) using 100 ng of each DNA sample. Final libraries
869 were quantifieded, checked on a Bioanalyzer 2100 (Agilent) and sequenced on a Illumina
870 Miseq system (2 × 150 paired end reads).
871
872 **Flow cytometry and EdU staining**
873 Nuclear DNA content was measured in leaves of 20-d-old seedlings, using the CyStain UV
874 Precise P Kit (Partec) according to the manufacturer's instructions. Nuclei were released in
875 nuclei extraction buffer (Partec) by chopping with a razor blade, stained with 4',6-diamidino-
876 2-phenylindole (DAPI) buffer and filtered through a 30 µM Celltrics mesh (Partec). Between
877 20,000 and 30,000 isolated nuclei were used for each ploidy level measurement using the
878 Attune Cytometer and the Attune Cytometer software (Life Technologies). At least four
879 independent biological replicates were analyzed. EdU staining was as described (Pedroza-
880 Garcia et al., 2016). For each root tip (n>10), the number of mitotic events was counted
881 directly under the microscope.
882
883 **Accession Numbers**
884 Sequence data from this article can be found in the Arabidopsis Genome Initiative or
885 GenBank/EMBL databases under the following accession numbers: *RADA*, At5g50340;
886 *RECG1*, At2g01440; *RECA2*, At2g19490; *RECA3*, At3g10140; *ANAC044*, At3g01600;
887 *ANAC085*, At5g14490; *KNOLLE*, At1g08560; *CDKB1;2*, At2g38620; *EHD2*, At4g05520; *PLE*,
888 At5g51600; *MYB3R3*, At3g09370; *MYB3R4*, At5g11510; *CYCD3;1*, At4g34160; *CYCD3;2*,
889 At5g67260; *CYCD3;3*, At3g50070; *MCM*2, At1g44900; *MCM3*, At5g46280; *PCNA1*,
890 At1g07370; *PCNA2*, At2g29270; *CDT1a*, At2g31270; *CycB1;1*, At4g37490; *WEE1*,
891 At1g02970; *BRCA1*, At4g21070 ; *RAD51*, At5g20850 ; *XRI1*, At5g48720; *SIM*, At5g04470;
892 *SMR1*, At3g10525; *SMR2*, At1g08180 ; *SMR3*, At5g02420; *SMR4*, At5g02220; *SMR5*,
893 At1g07500; *SMR6*, At5g40460; *SMR7*, At3g27630; *SMR8*, At1g10690; *SMR9*, At1g51355;
894 *SMR10*, At2g28870; *SMR11*, At2g28330; *SMR12*, At2g37610; *SMR13*, At5g59360; AOX1,
895 NM_001249237; RBCS, At1g67090.
896

897 **SUPPLEMENTAL DATA FILES**

898

899 **Supplemental Figure 1.** Phylogenetic distribution of RADA.

900

901 **Supplemental Figure 2.** Sequences alignment.

902

903 **Supplemental Figure 3.** Tissue-specific expression of Arabidopsis RADA.

904

905 **Supplemental Figure 4.** Effect of the point mutation K201A.

906

907 **Supplemental Figure 5.** Expression, purification and characterization of recombinant RADA.

908

909 **Supplemental Figure 6.** Transmission electron microscope (TEM) images.

910

911 **Supplemental Figure 7.** Pipeline cpDNA NGS analysis.

912

913 **Supplemental Table 1.** Oligonucleotides.

914

915

916 **Author Contributions**

917 NC, FW-L, CN, CR, MLR, ME and JMG performed research. NC, CR, MB, AD and JMG
918 designed the research and analyzed data. AF analyzed the Illumina sequences. NC and
919 JMG wrote the paper.

920

921 **Acknowledgments**

922 We are grateful to Dr. Sandra Noir for help with flow cytometry, to Dr. Esther Lechner for
923 vectors and technical advice and to Dr. Patrice Polard and Dr. Bénédicte Michel for helpful
924 discussions. This work has been published under the framework of the LABEX [ANR-11-
925 LABX-0057_MITOCROSS] and benefits from a funding from the state managed by the
926 French National Research Agency as part of the "Investments for the future" program.

927

928 ## References

929 **Abraham, R.T.** (2001). Cell cycle checkpoint signaling through the ATM and ATR kinases.
930 Genes Dev **15:** 2177-2196.
931 **Arrieta-Montiel, M.P., Shedge, V., Davila, J., Christensen, A.C., and Mackenzie, S.A.**
932 (2009). Diversity of the Arabidopsis mitochondrial genome occurs via nuclear-
933 controlled recombination activity. Genetics **183:** 1261-1268.
934 **Backert, S., Lynn Nielsen, B., and Börner, T.** (1997). The mystery of the rings: structure
935 and replication of mitochondrial genomes from higher plants. Trends in Plant Science
936 **2:** 477-483.
937 **Beam, C.E., Saveson, C.J., and Lovett, S.T.** (2002). Role for radA/sms in recombination
938 intermediate processing in Escherichia coli. J Bacteriol **184:** 6836-6844.
939 **Bendich, A.J.** (1996). Structural analysis of mitochondrial DNA molecules from fungi and
940 plants using moving pictures and pulsed-field gel electrophoresis. J. Mol. Biol. **255:**
941 564-588.
942 **Boesch, P., Weber-Lotfi, F., Ibrahim, N., Tarasenko, V., Cosset, A., Paulus, F.,**
943 **Lightowlers, R.N., and Dietrich, A.** (2011). DNA repair in organelles: Pathways,
944 organization, regulation, relevance in disease and aging. Biochim Biophys Acta **1813:**
945 186-200.
946 **Brenneman, M.A., Wagener, B.M., Miller, C.A., Allen, C., and Nickoloff, J.A.** (2002).
947 XRCC3 controls the fidelity of homologous recombination: roles for XRCC3 in late
948 stages of recombination. Mol Cell **10:** 387-395.
949 **Budar, F., Touzet, P., and De Paepe, R.** (2003). The nucleo-mitochondrial conflict in
950 cytoplasmic male sterilities revisited. Genetica **117:** 3-16.
951 **Carrie, C., Kuhn, K., Murcha, M.W., Duncan, O., Small, I.D., O'toole, N., and Whelan, J.**
952 (2009). Approaches to defining dual-targeted proteins in Arabidopsis. Plant Journal
953 **57:** 1128-1139.
954 **Christensen, A.C.** (2013). Plant mitochondrial genome evolution can be explained by DNA
955 repair mechanisms. Genome Biol Evol **5:** 1079-1086.
956 **Christensen, A.C.** (2018). Mitochondrial DNA Repair and Genome Evolution. In *Annual*
957 *Plant Reviews online*, pp. 11-32.
958 **Chun, J., Buechelmaier, E.S., and Powell, S.N.** (2013). Rad51 paralog complexes BCDX2
959 and CX3 act at different stages in the BRCA1-BRCA2-dependent homologous
960 recombination pathway. Mol Cell Biol **33:** 387-395.
961 **Cooper, D.L., Boyle, D.C., and Lovett, S.T.** (2015). Genetic analysis of Escherichia coli
962 RadA: functional motifs and genetic interactions. Mol. Microbiol. **95:** 769-779.
963 **Cooper, D.L., and Lovett, S.T.** (2016). Recombinational branch migration by the RadA/Sms
964 paralog of RecA in Escherichia coli. eLife **5**.
965 **Cox, M.M.** (2007). Motoring along with the bacterial RecA protein. Nat. Rev. Mol. Cell Biol. **8:**
966 127-138.
967 **Duan, S., Hu, L., Dong, B., Jin, H.L., and Wang, H.B.** (2020). Signaling from Plastid
968 Genome Stability Modulates Endoreplication and Cell Cycle during Plant
969 Development. Cell Rep **32:** 108019.
970 **Dubois, M., Selden, K., Bediee, A., Rolland, G., Baumberger, N., Noir, S., Bach, L.,**
971 **Lamy, G., Granier, C., and Genschik, P.** (2018). SIAMESE-RELATED1 Is
972 Regulated Posttranslationally and Participates in Repression of Leaf Growth under
973 Moderate Drought. Plant Physiol **176:** 2834-2850.
974 **Forget, A.L., and Kowalczykowski, S.C.** (2012). Single-molecule imaging of DNA pairing
975 by RecA reveals a three-dimensional homology search. Nature **482:** 423-427.
976 **Fuchs, P., Rugen, N., Carrie, C., Elsasser, M., Finkemeier, I., Giese, J., Hildebrandt,**
977 **T.M., Kuhn, K., Maurino, V.G., Ruberti, C., Schallenberg-Rudinger, M.,**
978 **Steinbeck, J., Braun, H.P., Eubel, H., Meyer, E.H., Muller-Schussele, S.J., and**
979 **Schwarzlander, M.** (2019). Single organelle function and organization as estimated
980 from Arabidopsis mitochondrial proteomics. Plant J 10.1111/tpj.14534.

Gualberto, J.M., and Newton, K.J. (2017). Plant Mitochondrial Genomes: Dynamics and Mechanisms of Mutation. Annu Rev Plant Biol **68:** 225-252.

Hanson, M.R., and Bentolila, S. (2004). Interactions of mitochondrial and nuclear genes that affect male gametophyte development. Plant Cell **16 Suppl:** S154-169.

Hudik, E., Yoshioka, Y., Domenichini, S., Bourge, M., Soubigout-Taconnat, L., Mazubert, C., Yi, D., Bujaldon, S., Hayashi, H., De Veylder, L., Bergounioux, C., Benhamed, M., and Raynaud, C. (2014). Chloroplast dysfunction causes multiple defects in cell cycle progression in the Arabidopsis crumpled leaf mutant. Plant Physiol **166:** 152-167.

Inoue, M., Fukui, K., Fujii, Y., Nakagawa, N., Yano, T., Kuramitsu, S., and Masui, R. (2017). The Lon protease-like domain in the bacterial RecA paralog RadA is required for DNA binding and repair. J Biol Chem **292:** 9801-9814.

Ishibashi, T., Isogai, M., Kiyohara, H., Hosaka, M., Chiku, H., Koga, A., Yamamoto, T., Uchiyama, Y., Mori, Y., Hashimoto, J., Ausio, J., Kimura, S., and Sakaguchi, K. (2006). Higher plant RecA-like protein is homologous to RadA. DNA Repair (Amst) **5:** 80-88.

Janska, H., Sarria, R., Woloszynska, M., Arrieta-Montiel, M., and Mackenzie, S.A. (1998). Stoichiometric shifts in the common bean mitochondrial genome leading to male sterility and spontaneous reversion to fertility. Plant Cell **10:** 1163-1180.

Langmead, B., and Salzberg, S.L. (2012). Fast gapped-read alignment with Bowtie 2. Nature Methods **9:** 357-U354.

Le Ret, M., Belcher, S., Graindorge, S., Wallet, C., Koechler, S., Erhardt, M., Williams-Carrier, R., Barkan, A., and Gualberto, J.M. (2018). Efficient Replication of the Plastid Genome Requires an Organellar Thymidine Kinase. PLANT PHYSIOLOGY **178:** 1643-1656.

Li, B., Fang, J., Singh, R.M., Zi, H., Lv, S., Liu, R., Dogra, V., and Kim, C. (2020). FATTY ACID DESATURASE5 Is Required to Induce Autoimmune Responses in Gigantic Chloroplast Mutants of Arabidopsis. Plant Cell **32:** 3240-3255.

Li, H., and Durbin, R. (2009). Fast and accurate short read alignment with Burrows-Wheeler transform. Bioinformatics **25:** 1754-1760.

Manchekar, M., Scissum-Gunn, K., Song, D., Khazi, F., Mclean, S.L., and Nielsen, B.L. (2006). DNA recombination activity in soybean mitochondria. J Mol Biol **356:** 288-299.

Marechal, A., Parent, J.S., Veronneau-Lafortune, F., Joyeux, A., Lang, B.F., and Brisson, N. (2009). Whirly proteins maintain plastid genome stability in Arabidopsis. Proc Natl Acad Sci U S A **106:** 14693-14698.

Maréchal, A., and Brisson, N. (2010). Recombination and the maintenance of plant organelle genome stability. New Phytologist **186:** 299-317.

Marie, L., Rapisarda, C., Morales, V., Bergé, M., Perry, T., Soulet, A.-L., Gruget, C., Remaut, H., Fronzes, R., and Polard, P. (2017). Bacterial RadA is a DnaB-type helicase interacting with RecA to promote bidirectional D-loop extension. Nature Communications **8:** 15638.

Melonek, J., Matros, A., Trosch, M., Mock, H.-P., and Krupinska, K. (2012). The Core of Chloroplast Nucleoids Contains Architectural SWIB Domain Proteins. The Plant Cell **24:** 3060-3073.

Meyer, E.H., Tomaz, T., Carroll, A.J., Estavillo, G., Delannoy, E., Tanz, S.K., Small, I.D., Pogson, B.J., and Millar, A.H. (2009). Remodeled respiration in ndufs4 with low phosphorylation efficiency suppresses Arabidopsis germination and growth and alters control of metabolism at night. Plant Physiol **151:** 603-619.

Miller-Messmer, M., Kuhn, K., Bichara, M., Le Ret, M., Imbault, P., and Gualberto, J.M. (2012). RecA-dependent DNA repair results in increased heteroplasmy of the Arabidopsis mitochondrial genome. Plant Physiol **159:** 211-226.

Mower, J.P., Touzet, P., Gummow, J.S., Delph, L.F., and Palmer, J.D. (2007). Extensive variation in synonymous substitution rates in mitochondrial genes of seed plants. BMC Evol. Biol. **7:** 135.

1036 **Nowack, M.K., Harashima, H., Dissmeyer, N., Zhao, X., Bouyer, D., Weimer, A.K., De**
1037 **Winter, F., Yang, F., and Schnittger, A.** (2012). Genetic framework of cyclin-
1038 dependent kinase function in Arabidopsis. Dev Cell **22:** 1030-1040.
1039 **Odahara, M., Masuda, Y., Sato, M., Wakazaki, M., Harada, C., Toyooka, K., and Sekine,**
1040 **Y.** (2015). RECG maintains plastid and mitochondrial genome stability by
1041 suppressing extensive recombination between short dispersed repeats. PLoS Genet
1042 **11:** e1005080.
1043 **Owusu-Ansah, E., Yavari, A., Mandal, S., and Banerjee, U.** (2008). Distinct mitochondrial
1044 retrograde signals control the G1-S cell cycle checkpoint. Nature Genetics **40:** 356-
1045 361.
1046 **Pedroza-Garcia, J.A., Domenichini, S., Mazubert, C., Bourge, M., White, C., Hudik, E.,**
1047 **Bounon, R., Tariq, Z., Delannoy, E., Del Olmo, I., Pineiro, M., Jarillo, J.A.,**
1048 **Bergounioux, C., Benhamed, M., and Raynaud, C.** (2016). Role of the Polymerase
1049 sub-unit DPB2 in DNA replication, cell cycle regulation and DNA damage response in
1050 Arabidopsis. Nucleic Acids Res **44:** 7251-7266.
1051 **Pedroza-Garcia, J.A., Najera-Martinez, M., Mazubert, C., Aguilera-Alvarado, P., Drouin-**
1052 **Wahbi, J., Sanchez-Nieto, S., Gualberto, J.M., Raynaud, C., and Plasencia, J.**
1053 (2019). Role of pyrimidine salvage pathway in the maintenance of organellar and
1054 nuclear genome integrity. Plant J **97:** 430-446.
1055 **Peres, A., Churchman, M.L., Hariharan, S., Himanen, K., Verkest, A., Vandepoele, K.,**
1056 **Magyar, Z., Hatzfeld, Y., Van Der Schueren, E., Beemster, G.T., Frankard, V.,**
1057 **Larkin, J.C., Inze, D., and De Veylder, L.** (2007). Novel plant-specific cyclin-
1058 dependent kinase inhibitors induced by biotic and abiotic stresses. J Biol Chem **282:**
1059 25588-25596.
1060 **Qing, Y., Yamazoe, M., Hirota, K., Dejsuphong, D., Sakai, W., Yamamoto, K.N., Bishop,**
1061 **D.K., Wu, X., and Takeda, S.** (2011). The epistatic relationship between BRCA2 and
1062 the other RAD51 mediators in homologous recombination. PLoS Genet **7:** e1002148.
1063 **Quinlan, A.R., and Hall, I.M.** (2010). BEDTools: a flexible suite of utilities for comparing
1064 genomic features. Bioinformatics **26:** 841-842.
1065 **Ragunathan, K., Liu, C., and Ha, T.** (2012). RecA filament sliding on DNA facilitates
1066 homology search. eLife **1:** e00067.
1067 **Riou-Khamlichi, C., Menges, M., Healy, J.M., and Murray, J.A.** (2000). Sugar control of
1068 the plant cell cycle: differential regulation of Arabidopsis D-type cyclin gene
1069 expression. Mol Cell Biol **20:** 4513-4521.
1070 **Sabar, M., Balk, J., and Leaver, C.J.** (2005). Histochemical staining and quantification of
1071 plant mitochondrial respiratory chain complexes using blue-native polyacrylamide gel
1072 electrophoresis. Plant J **44:** 893-901.
1073 **Shedge, V., Arrieta-Montiel, M., Christensen, A.C., and Mackenzie, S.A.** (2007). Plant
1074 mitochondrial recombination surveillance requires unusual RecA and MutS homologs.
1075 Plant Cell **19:** 1251-1264.
1076 **Slade, D., Lindner, A.B., Paul, G., and Radman, M.** (2009). Recombination and replication
1077 in DNA repair of heavily irradiated Deinococcus radiodurans. Cell **136:** 1044-1055.
1078 **Sloan, D.B.** (2013). One ring to rule them all? Genome sequencing provides new insights
1079 into the 'master circle' model of plant mitochondrial DNA structure. New Phytologist
1080 **200:** 978-985.
1081 **Sloan, D.B., Wu, Z., and Sharbrough, J.** (2018). Correction of Persistent Errors in
1082 Arabidopsis Reference Mitochondrial Genomes. Plant Cell **30:** 525-527.
1083 **Small, I., Suffolk, R., and Leaver, C.J.** (1989). Evolution of plant mitochondrial genomes via
1084 substoichiometric intermediates. Cell **58:** 69-76.
1085 **Stupar, R.M., Lilly, J.W., Town, C.D., Cheng, Z., Kaul, S., Buell, C.R., and Jiang, J.**
1086 (2001). Complex mtDNA constitutes an approximate 620-kb insertion on Arabidopsis
1087 thaliana chromosome 2: implication of potential sequencing errors caused by large-
1088 unit repeats. Proc Natl Acad Sci U S A **98:** 5099-5103.

1089 **Takahashi, N., Ogita, N., Takahashi, T., Taniguchi, S., Tanaka, M., Seki, M., and Umeda,**
1090 **M.** (2019). A regulatory module controlling stress-induced cell cycle arrest in
1091 Arabidopsis. eLife **8**.
1092 **Touzet, P., and Meyer, E.H.** (2014). Cytoplasmic male sterility and mitochondrial
1093 metabolism in plants. Mitochondrion **19 Pt B:** 166-171.
1094 **Trolet, A., Baldrich, P., Criqui, M.C., Dubois, M., Clavel, M., Meyers, B.C., and**
1095 **Genschik, P.** (2019). Cell Cycle-Dependent Regulation and Function of
1096 ARGONAUTE1 in Plants. Plant Cell **31:** 1734-1750.
1097 **Vermel, M., Guermann, B., Delage, L., Grienenberger, J.M., Marechal-Drouard, L., and**
1098 **Gualberto, J.M.** (2002). A family of RRM-type RNA-binding proteins specific to plant
1099 mitochondria. Proc Natl Acad Sci U S A **99:** 5866-5871.
1100 **Vitart, V., Depaepe, R., Mathieu, C., Chetrit, P., and Vedel, F.** (1992). Amplification of
1101 substoichiometric recombinant mitochondrial DNA sequences in a nuclear, male
1102 sterile mutant regenerated from protoplast culture in Nicotiana sylvestris. Mol. Gen.
1103 Genet. **233:** 193-200.
1104 **Wallet, C., Le Ret, M., Bergdoll, M., Bichara, M., Dietrich, A., and Gualberto, J.M.** (2015).
1105 The RECG1 DNA Translocase Is a Key Factor in Recombination Surveillance,
1106 Repair, and Segregation of the Mitochondrial DNA in Arabidopsis. Plant Cell **27:**
1107 2907-2925.
1108 **Weimer, A.K., Biedermann, S., Harashima, H., Roodbarkelari, F., Takahashi, N.,**
1109 **Foreman, J., Guan, Y., Pochon, G., Heese, M., Van Damme, D., Sugimoto, K.,**
1110 **Koncz, C., Doerner, P., Umeda, M., and Schnittger, A.** (2016). The plant-specific
1111 CDKB1-CYCB1 complex mediates homologous recombination repair in Arabidopsis.
1112 EMBO J **35:** 2068-2086.
1113 **West, S.C.** (1997). Processing of recombination intermediates by the RuvABC proteins.
1114 Annu Rev Genet **31:** 213-244.
1115 **Whitby, M.C., Vincent, S.D., and Lloyd, R.G.** (1994). Branch migration of Holliday
1116 junctions: identification of RecG protein as a junction specific DNA helicase. EMBO J
1117 **13:** 5220-5228.
1118 **Wittig, I., Braun, H.P., and Schägger, H.** (2006). Blue native PAGE. Nat Protoc **1:** 418-428.
1119 **Woloszynska, M., and Trojanowski, D.** (2009). Counting mtDNA molecules in Phaseolus
1120 vulgaris: sublimons are constantly produced by recombination via short repeats and
1121 undergo rigorous selection during substoichiometric shifting. Plant Mol Biol **70:** 511-
1122 521.
1123 **Xu, Y.Z., Santamaria Rde, L., Virdi, K.S., Arrieta-Montiel, M.P., Razvi, F., Li, S., Ren, G.,**
1124 **Yu, B., Alexander, D., Guo, L., Feng, X., Dweikat, I.M., Clemente, T.E., and**
1125 **Mackenzie, S.A.** (2012). The chloroplast triggers developmental reprogramming
1126 when mutS HOMOLOG1 is suppressed in plants. Plant Physiol **159:** 710-720.
1127 **Yi, D., Alvim Kamei, C.L., Cools, T., Vanderauwera, S., Takahashi, N., Okushima, Y.,**
1128 **Eekhout, T., Yoshiyama, K.O., Larkin, J., Van Den Daele, H., Conklin, P., Britt,**
1129 **A., Umeda, M., and De Veylder, L.** (2014). The Arabidopsis SIAMESE-RELATED
1130 cyclin-dependent kinase inhibitors SMR5 and SMR7 regulate the DNA damage
1131 checkpoint in response to reactive oxygen species. Plant Cell **26:** 296-309.
1132 **Yoshiyama, K.O., Kobayashi, J., Ogita, N., Ueda, M., Kimura, S., Maki, H., and Umeda,**
1133 **M.** (2013). ATM-mediated phosphorylation of SOG1 is essential for the DNA damage
1134 response in Arabidopsis. EMBO Rep **14:** 817-822.
1135 **Yoshiyama, K.O.** (2016). SOG1: a master regulator of the DNA damage response in plants.
1136 Genes Genet Syst **90:** 209-216.
1137 **Zaegel, V., Guermann, B., Le Ret, M., Andres, C., Meyer, D., Erhardt, M., Canaday, J.,**
1138 **Gualberto, J.M., and Imbault, P.** (2006). The plant-specific ssDNA binding protein
1139 OSB1 is involved in the stoichiometric transmission of mitochondrial DNA in
1140 Arabidopsis. Plant Cell **18:** 3548-3563.
1141 **Zampini, E., Lepage, E., Tremblay-Belzile, S., Truche, S., and Brisson, N.** (2015).
1142 Organelle DNA rearrangement mapping reveals U-turn-like inversions as a major
1143 source of genomic instability in Arabidopsis and humans. Genome Res **25:** 645-654.

1144 # FIGURE LEGENDS

1145 **Figure 1. Arabidopsis RADA is targeted to both chloroplasts and mitochondria.**

1146 (**A** and **B)** Intracellular localization of RADA:GFP fusion proteins constitutively expressed in
1147 Arabidopsis transgenic plants. Both the full length protein (RADA:GFP) or just its N-terminal
1148 part (N-RADA:GFP) drive localization into chloroplasts (co-localization with autofluorescence
1149 of chlorophyll) and into mitochondria (characteristic cytosolic speckles). In chloroplasts
1150 RADA:GFP is predominant in dots that could be nucleoids (insert in A). (**C**) Confirmation of
1151 co-localization with red fluorescence of MitoTracker. (**D**) Co-localization with plastidial
1152 nucleoid marker PEND:dsRED, after biolistic co-transfection in *Nicotiana benthamiana*
1153 leaves.

1154

1155 **Figure 2. The Arabidopsis RADA is structurally and functionally homologous to**
1156 **bacterial RadA.**

1157 (**A**) The modular structure of plant RADA is similar to the one from bacteria, with a N-terminal
1158 zinc-finger (C4), a helicase domain and a Lon-protease-like domain (H and P domains,
1159 respectively). Plant precursor proteins have an N-terminal extension containing an organellar
1160 targeting sequence (OTS). (**B**) Model of Arabidopsis RADA superposed on the known
1161 structure of *S. pneumoniae* RadA (in gray) (Marie et al., 2017). The color code of relevant
1162 domains is as in (A). A bound ADP (stick representation) and the Mg^{2+} ion (yellow ball) are
1163 shown. (**C**) Complementation of an *E. coli radA* mutant (ΔRadA) for growth in the presence of
1164 genotoxic ciprofloxacin (CIP). Arabidopsis *RADA* (*At*-RADA) complements the mutation as
1165 efficiently as the bacterial protein (*Ec*-RadA) cloned in the same expression vector.

1166

1167 **Figure 3. RADA preferentially binds ssDNA**.

1168 (**A**) EMSA experiments showing that RADA binds any ssDNA-containing DNA structure with
1169 higher affinity than dsDNA. Lower and higher molecular weigh complexes are indicated by
1170 white and black arrowheads respectively. A predominant band seen with the 5'-overhang
1171 probe is artefactual, already present in the absence of protein. (**B**) Analysis on low
1172 concentration gel (4.5 % as compared to 8 % in A) of the formation of a high-molecular
1173 weight RADA filament on ssDNA, which is promoted by ATP or ADP (1 mM). The K201A
1174 mutant protein binds ssDNA with an affinity comparable to the one of the WT protein.
1175 Increasing concentrations of RADA or of K201A used in (A) and (B) are indicated by the grey
1176 triangles. (**C**) Competition experiments. A 30-mer ssDNA oligonucleotide (7x[AGTC]AG) was
1177 used as probe in EMSA experiments with recombinant RADA, and sequence specificity was
1178 tested by competition with increasing concentrations of the cold homologous oligonucleotide

1179 or with 30-oligomers (poly-dA, pol-dT, poly-dC and poly-dG). Quantification of the results is
1180 shown on the right. Only poly-dA showed reduced competition for RADA binding to ssDNA.
1181
1182 **Figure 4. Branch-migration activities of RADA.**
1183 (**A**) In an *in vitro* strand-invasion reaction recombinant RADA accelerates branch-migration of
1184 DNA heteroduplexes initiated by RecA. An explanation of the different substrates and
1185 products is shown. (**B**) Ratio of final product as compared to the initial linear dsDNA
1186 substrate in 6 independent experiments, showing that in the presence of RADA there is
1187 faster resolution of branched intermediates. (**C**) Experiment showing that RADA alone can
1188 finalize branch-migration initiated by RecA: a reaction at t=7 min was arrested by
1189 deproteination (left panel) and the DNA purified. Without further addition of RecA or RADA
1190 proteins there is no spontaneous progression of the reaction (middle panel), but added
1191 RADA can alone resolve the recombination intermediates into the final product (right panel).
1192 (**D**) RADA alone cannot initiate strand invasion. (**E**) Mutation of the ATPase Walker domain
1193 of RADA (K201A) inhibits the reaction.
1194
1195 **Figure 5. Arabidopsis *radA* mutants and phenotypes.**
1196 (**A**) Schematic representation of the Arabidopsis *RADA* gene. Coding sequences are in black
1197 and 5'- and 3'-UTRs are in gray. The position of the T-DNA insertions in *radA* mutant lines is
1198 shown. (**B**) *radA* plants show severe growth retardation, with distorted leaves presenting
1199 chlorotic sectors. These phenotypes can be complemented by expression of HA-tagged
1200 RADA (RADA:HA) under control of the endogenous *pRADA* promoter. (**C**) root shortening of
1201 *radA* plants. (**D**) Detail of leaf phenotype. (**E**) 4-month old *radA-1* plant grown under short
1202 days (8h light), showing perennial vegetative growth with development of aerial rosettes.
1203
1204 **Figure 6. Reduced fertility of *radA* plants.**
1205 (**A**) Comparison of WT and *radA* flower stems showing very small *radA* siliques. (**B**) *radA*
1206 siliques mostly contain aborted seeds, and most of the few seeds produced are non-viable.
1207 (**C**) Alexander staining of pollen in *radA* anthers as compared to WT, showing little pollen
1208 production and an abundance of small and aberrant pollen grains (indicated by arrows). (**D**)
1209 Visible and SEM Images showing that in *radA* no pollen binds to the papillae of the stigma.
1210 (**E**) Differential interference contrast images of ovules in crosses between *radA-1* flowers and
1211 WT pollen. Black arrowheads indicate central cell and egg cell nuclei in unfertilized ovules.
1212 White arrowheads indicate developing embryos in fertilized ovules, at the 2 up to 8 cells
1213 globular stage, three days after pollination (DAP). Only 16 % of *radA* ovules could be
1214 fertilized. Scale bar is 50 µm. (**F**) At seven DAP the pollinated pistils did not develop further.
1215

1216 **Figure 7. Changes in mtDNA sequences stoichiometry in *radA* mutants because of**
1217 **increased ectopic recombination across repeats.**
1218 (**A**) Picture of severely affected (*radA-1*#1 and *radA-2*#1) and mildly affected (*radA-1*#2 and
1219 *radA-2*#2) seedlings. (**B**) Scanning of their mtDNA for changes in relative copy numbers of
1220 the different mtDNA regions. Sequences spaced 5-10 kb apart on the mtDNA were quantified
1221 by qPCR. Coordinates are those of the Col-0 mtDNA sequence. The position of the mtDNA
1222 large repeats LR1 and LR2 and of relevant intermediate size repeats are shown below the
1223 graphic. Regions with changed stoichiometry flanked by repeat pairs are shadowed. (**C**)
1224 Accumulation of crossover products from mtDNA repeats L, F and EE in *radA* seedlings as
1225 compared to WT. Results are in a log2 scale. The scheme above shows the qPCR relative
1226 quantification of parental sequences 1/1 and 2/2 and of the corresponding crossover
1227 products 1/2 and 2/1. Results are the mean of three technical replicates, and error bars
1228 correspond to *SD* values.
1229
1230 **Figure 8. No significant effect of the *radA* mutation on the stability of the plastidial**
1231 **genome.**
1232 The DNA from a leaf of four independent 4-week-old *radA-1* plants and of two WT plants was
1233 extracted and sequenced on a MySeq Illumina system (2x150 bp paired-end). The reads
1234 corresponding to the cpDNA were extracted and investigated for possible changes in cpDNA
1235 stability. (**A**) Normalized cpDNA coverage, showing comparable copy number of the cpDNA
1236 in WT and in *radA*, and no apparent changes in sequences stoichiometry. A schematic
1237 representation of the cpDNA is shown above, indicating the large and small single-copy
1238 regions (LSC and SSC, respectively) and a single copy of the inverted repeated region (IR).
1239 (**B**) Abundance of reads identified as corresponding to rearranged cpDNA molecules (see
1240 supplemental figure 7 for a scheme of the analysis pipeline). A slight increase, up to two-fold
1241 as compared to WT, was identified in the *radA* plants.
1242
1243 **Figure 9. Hemicomplementation of *radA***
1244 (**A**) Schematic representation of the constructs used for testing hemicomplementation of the
1245 *radA* phenotypes, with a construct only targeting RADA to mitochondria, by fusion to the
1246 targeting sequence of alternative oxidase (AOX1) and with a construct only targeting RADA
1247 to plastids, by fusion to the targeting sequence of the small subunit of Rubisco (RBCS).
1248 (**B**) Growth phenotypes of four-week-old hemicomplemented plants in a segregating T2
1249 population as compared to WT and *radA-1*. Only partial complementation was observed with
1250 the AOX1:RADA construct, but plants complemented with the RBCS:RADA construct
1251 showed little or no complementation. (**C**) Relative quantification of the accumulation of

1252 crossover product L-1/2, resulting from ectopic recombination involving mitochondrial pair of
1253 repeats L in *radA-1* and in hemicomplemented plants (log2 scale).
1254
1255 **Figure 10. Synergistic effects of the *radA* mutation on *recG1* and *recA3*.**
1256 (**A**) Crosses of *recG1-2* and *radA-1* (pollen donor) show that double homozygote *recG1 radA*
1257 plants are not more affected in their development than simple homozygote *radA* plants.
1258 (**B**) qPCR analysis of the copy number of mtDNA sequences around and within the region
1259 comprised between the pair of repeats EE, previously shown to generate an episome by
1260 recombination in *recG1* plants (Wallet et al., 2015). Autonomous replication of the episome is
1261 significantly increased in the *recG1 radA* double mutant. Results show the mean and *SD*
1262 error bars from 2 or 3 (for *recG1 radA*) biological replicates. (**C**) Double homozygote
1263 *recA3 radA* seedlings do not grow roots and do not grow further. The phenotype is similar to
1264 the one observed for *recA2* mutants (Miller-Messmer et al., 2012). The scale bar is 1 mm.
1265 (**D**) Scanning of the copy numbers of the different mtDNA regions, as described in Figure 7,
1266 in pools of *recA3 radA* double mutant seedlings. Results were compared to those of WT
1267 seedling of same size, and are represented in log scale. Sequences that are also present in
1268 the nuclear genome of Col-0 are shaded yellow in the mtDNA representation.
1269
1270 **Figure 11. Accumulation of mitochondrial transcripts in *radA*.**
1271 **(A)** Representative mitochondrial transcripts were quantified by RT-qPCR, from the RNA of
1272 10-day-old seedlings grown *in vitro,* and normalized against a set of nuclear housekeeping
1273 genes. The quantification of several orf transcripts whose expression could be potentially
1274 affected by ectopic recombination involving IRs is shown on the right, in red. Results are on a
1275 log2 scale and are the mean from four biological replicates (two pools of *radA-1* and two
1276 pools of *radA-2* seedlings) with the corresponding *SD* error bars. **(B)** Chimeric *orf195* and
1277 *orf315* created by recombination whose transcription is augmented in *radA* plants. The
1278 regions corresponding to *rps3* and *atp9* sequences are shown in blue. Repeated sequences
1279 are represented by orange bars. Coordinates on the mtDNA are indicated. (**C**) Blue-Native
1280 gel analysis of WT and *radA* purified mitochondria. 80 µg of proteins were loaded in each
1281 well, and run in parallel with size markers (High Molecular Weight Calibration Kit, GE
1282 Healthcare). Coomassie staining, complex I activity staining and immunodetection of
1283 complex III (with a cytochrome c1-specific antibody) revealed no apparent changes in *radA*
1284 respiratory complexes. The white arrowheads indicate green-yellow bands that were already
1285 visible before staining and likely corresponded to plastidial contamination. The black
1286 arrowhead indicates the complex I activity band.
1287
1288

1289 **Figure 12. Cell cycle progression is impaired in *radA* plants.**
1290 **(A)** Scanning electron microscopy images showing much larger epidermal cells and fewer
1291 stomata in *radA* leaves. Scale bar is 20 µm. **(B)** Flow-cytometry profiles obtained in WT (Col-
1292 0) and *radA.* The DNA content of nuclei extracted from the first true leaves of 20-day-old
1293 plants was analyzed. **(C)** Ploidy distribution, showing decreased endoreduplication in the
1294 mutant, with an increased proportion of 4C and 8C nuclei and a decreased proportion of 16C
1295 nuclei. Values are the average ± *SD* of 4 experiments for WT and six experiments for *radA*
1296 (n>20 000 nuclei). **(D)** Decreased DNA synthesis in the nuclei of *radA* root tip cells, as
1297 evaluated by the ratio between EdU positive and DAPI (4',6'-diamidino-2-phénylindol)
1298 positive cells. **(E)** Decreased number of cells undergoing mitosis. Significances were
1299 calculated by Student's t test. **(F)** RT-qPCR analysis of the expression of a set of cell cycle
1300 related genes in 10-day-old WT and *radA* seedlings, revealing significant activation of *SMR5*
1301 and *ANAC085*. The data is represented in a log2 scale and is the mean ± *SD* of three
1302 biological replicates (two pools of seedlings from *radA-1* and one from *radA-2*). **(G)** NBT
1303 (nitro blue tetrazolium) staining for O^{2-} in plants of equivalent size grown under the same
1304 conditions, showing that *radA* mutants accumulate much more ROS than WT plants. Scale
1305 bar is 1 cm. **(H)** The expression of several cell cycle-related genes is suppressed by the ROS
1306 quencher ascorbic acid (1 mM), both in WT and in *radA* 10-day-old seedlings.
1307
1308 **Figure 13. Model for possible retrograde regulation by organellar DNA instability**
1309 Possible retrograde effect of the instability of organellar genomes on the expression of cell-
1310 cycle regulators inhibiting plant growth and development. The release of ROS from
1311 mitochondria and/or chloroplast could be the signal transmitted to the nucleus.
1312

1313

1314 **Supplemental Figure 1.** Phylogenetic distribution of RADA.

1315 Genes coding for RadA-like proteins are found in all bacteria, in land plants, green, brown
1316 and red algae, diatoms and other organisms of the Stramenopile group. *Arabidopsis thaliana,*
1317 NP_199845; *Populus trichocarpa,* EEE84551; *Vitis vinifera,* XP_002277638; *Oryza sativa,*
1318 NP_001056828; *Zea mays,* NP_001170708; *Selaginella moellendorffii,* XP_002976563;
1319 *Physcomitrella patens,* XP_001757578; *Ostreococcus tauri,* XP_003084463; *Coccomyxa*
1320 *subellipsoidea,* XP_005643141; *Chlorella variabilis,* EFN56488; *Cyanidioschyzon merolae,*
1321 XP_005536634; *Galdieria sulphuraria,* XP_005709405; *Ectocarpus siliculosus,* CBJ25917;
1322 *Phaeodactylum tricornutum,* XP_002178713; *Thalassiosira oceanica,* EJK58798;
1323 *Saprolegnia diclina,* EQC30001; *Phytophthora infestans,* XP_002904225; *Myxococcus*
1324 *xanthus,* YP_629513; *Rickettsia prowazekii,* WP_014607237; *Neisseria meningitidis,*
1325 WP_002258526; *Escherichia coli,* WP_001458566; *Microcystis aeruginosa,* WP_002742386;
1326 *Synechocystis sp,* WP_009633429; *Geminocystis herdmanii,* WP_017296205; *Bacillus*
1327 *anthracis,* NP_842650; *Amphibacillus jilinensis,* WP_017473696.

1328

1329 **Supplemental Figure 2.** Sequence alignment.

1330 Sequence alignment between representative land plant RADA sequences and RadA from
1331 proteobacteria and cyanobacteria. The Zinc-finger and KNRFG RadA-specific motif are
1332 shaded in yellow and blue respectively, and the Walker A and B motifs in green.

1333

1334 **Supplemental Figure 3.** Tissue-specific expression of Arabidopsis *RADA*.

1335 (**A**) Results extracted from Genevestigator (https://genevestigator.com/) (**B**) promoter-GUS
1336 fusion results, showing predominant expression in very young leaves, in sepals, in anthers
1337 filament and in the stigmata.

1338

1339 **Supplemental Figure 4.** Effect of the point mutation K201A.

1340 Effect of the point mutation K201A (amino acids in green) on the Walker A domain of RadA
1341 in the binding and hydrolysis of ATP. The structure shown is the one from bacterial RadA
1342 (Marie et al. 2017), with bound ADP and Mg^{2+} ion (sphere). The two phosphate groups of
1343 ADP are in red.

1344

1345 **Supplemental Figure 5.** Expression, purification and characterization of recombinant RADA.

1346 The Arabidopsis RADA sequence minus the first 48 codons corresponding to the OTS was
1347 cloned in the expression vector pET28a fused to a N-terminal His-tag. The recombinant
1348 RADA and Walker mutant K201A were expressed in the Rosetta(DE3) strain and purified by
1349 affinity and gel filtration. (**A**) Coomassie gel staining analysis of the recombinant proteins. (**B**)

1350 Gel filtration on Superdex S200 showed that RADA purified as two peaks of high molecular
1351 weight. (**C**) Dynamic light scattering of the protein fraction from peak 2 shows that it is
1352 monodispersed and corresponding to a size of about 340 kDa, which is consistent with a
1353 hexameric RADA molecule. (**D**) EMSA analysis of the binding to an ssDNA oligonucleotide.
1354 Fractions corresponding to both peaks give complexes of the same size, although fractions
1355 of peak 1 give predominantly higher molecular weight complexes.
1356
1357 **Supplemental Figure 6.** Transmission electron microscope (TEM) images
1358 TEM images of cells from leaves of same size showed morphologically normal chloroplasts
1359 (cp) in *radA.* Mitochondria (mt) were enlarged and less electron dense as compared to
1360 mitochondria from WT cells.
1361
1362 **Supplemental Figure 7.** Pipeline cpDNA NGS analysis.
1363 Schematic representation of the analysis workflow of Illumina sequences for identification of
1364 cpDNA rearrangements. Blue background boxes represent text manipulation steps, while
1365 yellow and red background ones symbolize quality filtering and mapping, respectively.
1366 Sequencing was performed on both ends of DNA fragments (R1 and R2). BWA: Burrows-
1367 Wheeler Aligner. R1 & R2: Paired-end sequencing read1 and read2.
1368

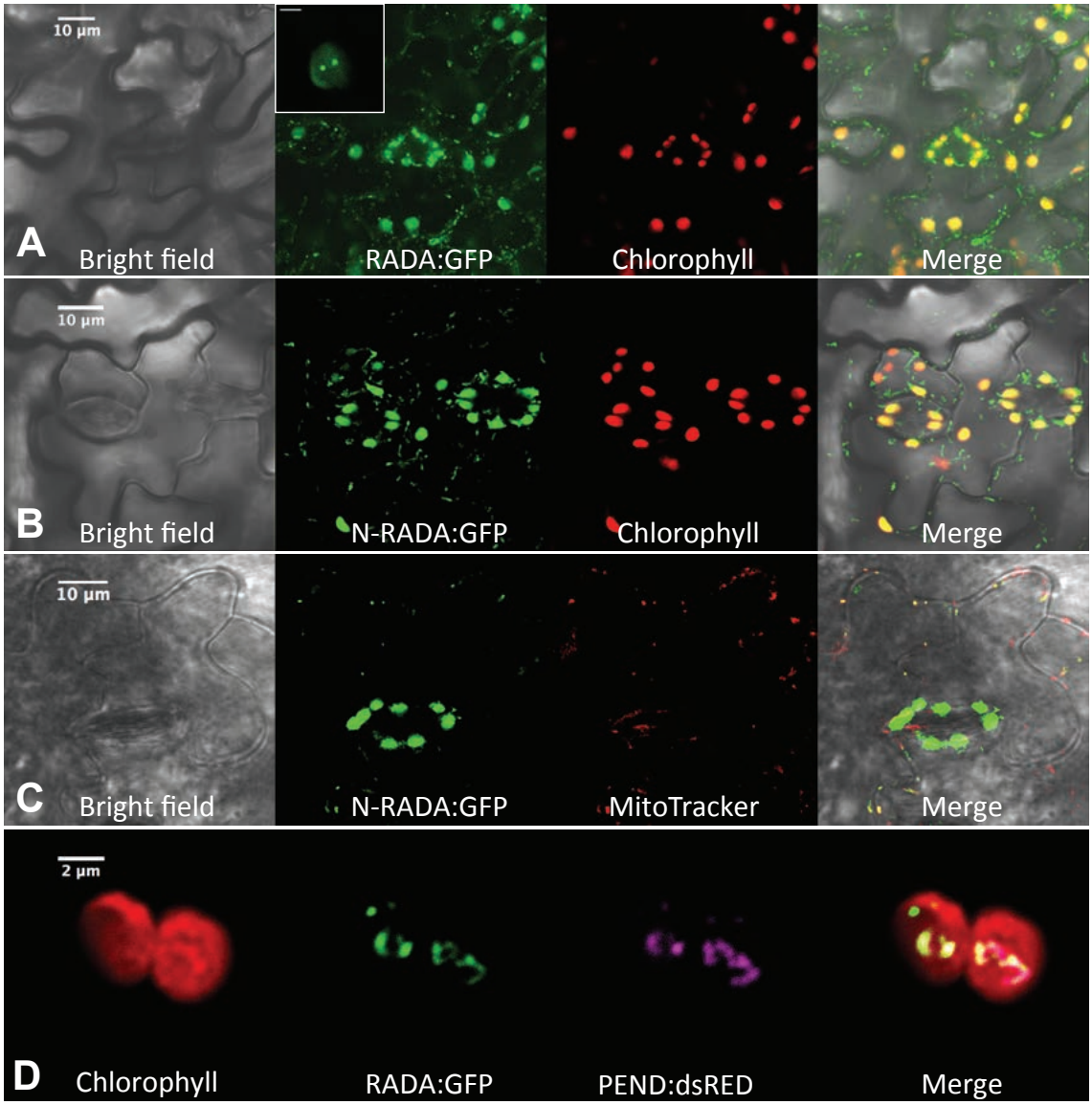

Figure 1. Arabidopsis RADA is targeted to both chloroplasts and mitochondria.
(**A** and **B)** Intracellular localization of RADA:GFP fusion proteins constitutively expressed in Arabidopsis transgenic plants. Both the full length protein (RADA:GFP) or just its N-terminal part (N-RADA:GFP) drive localization into chloroplasts (co-localization with autofluorescence of chlorophyll) and into mitochondria (characteristic cytosolic speckles). In chloroplasts RADA:GFP is predominant in dots that could be nucleoids (insert in A). (**C**) Confirmation of co-localization with red fluorescence of MitoTracker. (**D**) Co-localization with plastidial nucleoid marker PEND:dsRED, after biolistic co-transfection in *Nicotiana benthamiana* leaves.

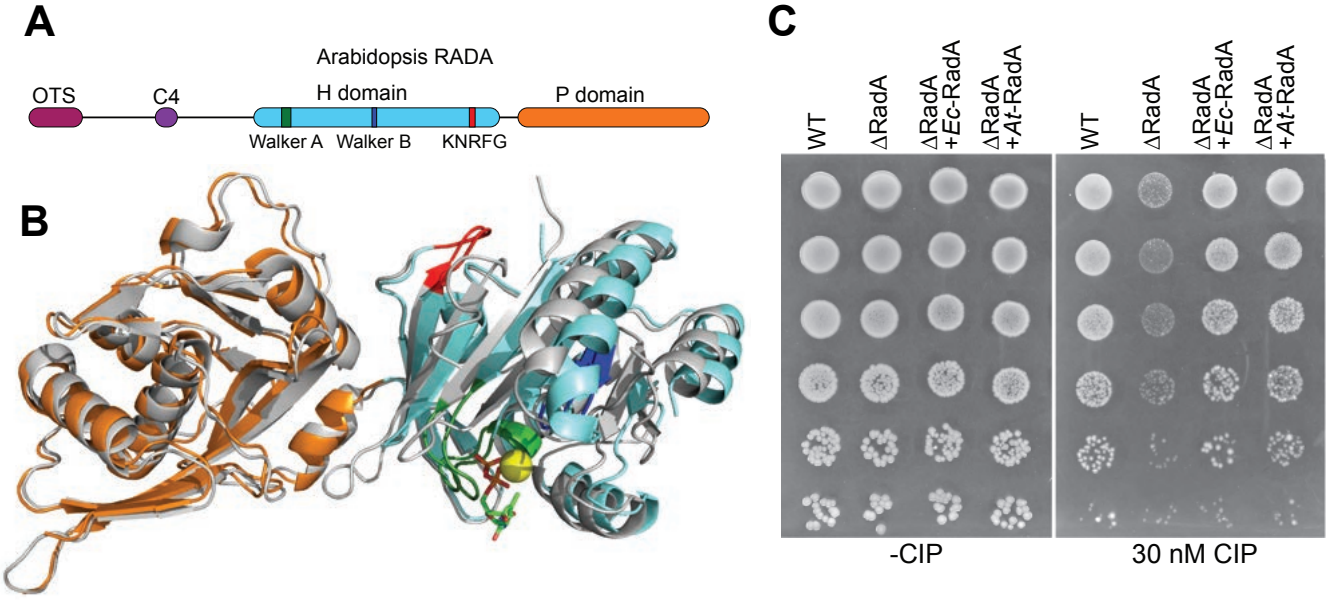

Figure 2. The Arabidopsis RADA is structurally and functionally homologous to bacterial RadA.

(**A**) The modular structure of plant RADA is similar to the one from bacteria, with a N-terminal zinc-finger (C4), a helicase domain and a Lon-protease-like domain (H and P domains, respectively). Plant precursor proteins have an N-terminal extension containing an organellar targeting sequence (OTS). (**B**) Model of Arabidopsis RADA superposed on the known structure of *S. pneumoniae* RadA (in gray) (Marie et al., 2017). The color code of relevant domains is as in (A). A bound ADP (stick representation) and the Mg^{2+} ion (yellow ball) are shown. (**C**) Complementation of an *E. coli radA* mutant (ΔRadA) for growth in the presence of genotoxic ciprofloxacin (CIP). Arabidopsis *RADA* (*At*-RADA) complements the mutation as efficiently as the bacterial protein (*Ec*-RadA) cloned in the same expression vector.

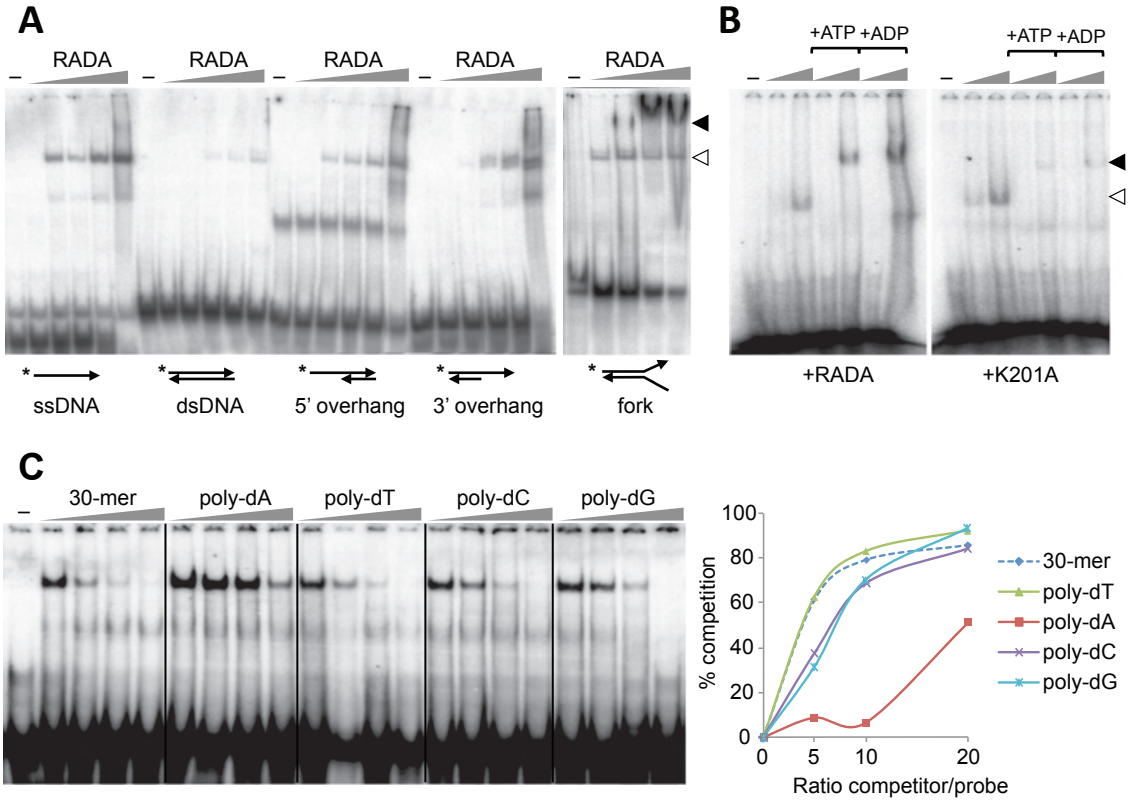

Figure 3. RADA preferentially binds ssDNA.
(**A**) EMSA experiments showing that RADA binds any ssDNA-containing DNA structure with higher affinity than dsDNA. Lower and higher molecular weigh complexes are indicated by white and black arrowheads respectively. A predominant band seen with the 5'-overhang probe is artefactual, already present in the absence of protein. (**B**) Analysis on low concentration gel (4.5 % as compared to 8 % in A) of the formation of a high-molecular weight RADA filament on ssDNA, which is promoted by ATP or ADP (1 mM). The K201A mutant protein binds ssDNA with an affinity comparable to the one of the WT protein. Increasing concentrations of RADA or of K201A used in (A) and (B) are indicated by the grey triangles. (**C**) Competition experiments. A 30-mer ssDNA oligonucleotide (7x[AGTC]AG) was used as probe in EMSA experiments with recombinant RADA, and sequence specificity was tested by competition with increasing concentrations of the cold homologous oligonucleotide or with 30-oligomers (poly-dA, pol-dT, poly-dC and poly-dG). Quantification of the results is shown on the right. Only poly-dA showed reduced competition for RADA binding to ssDNA.

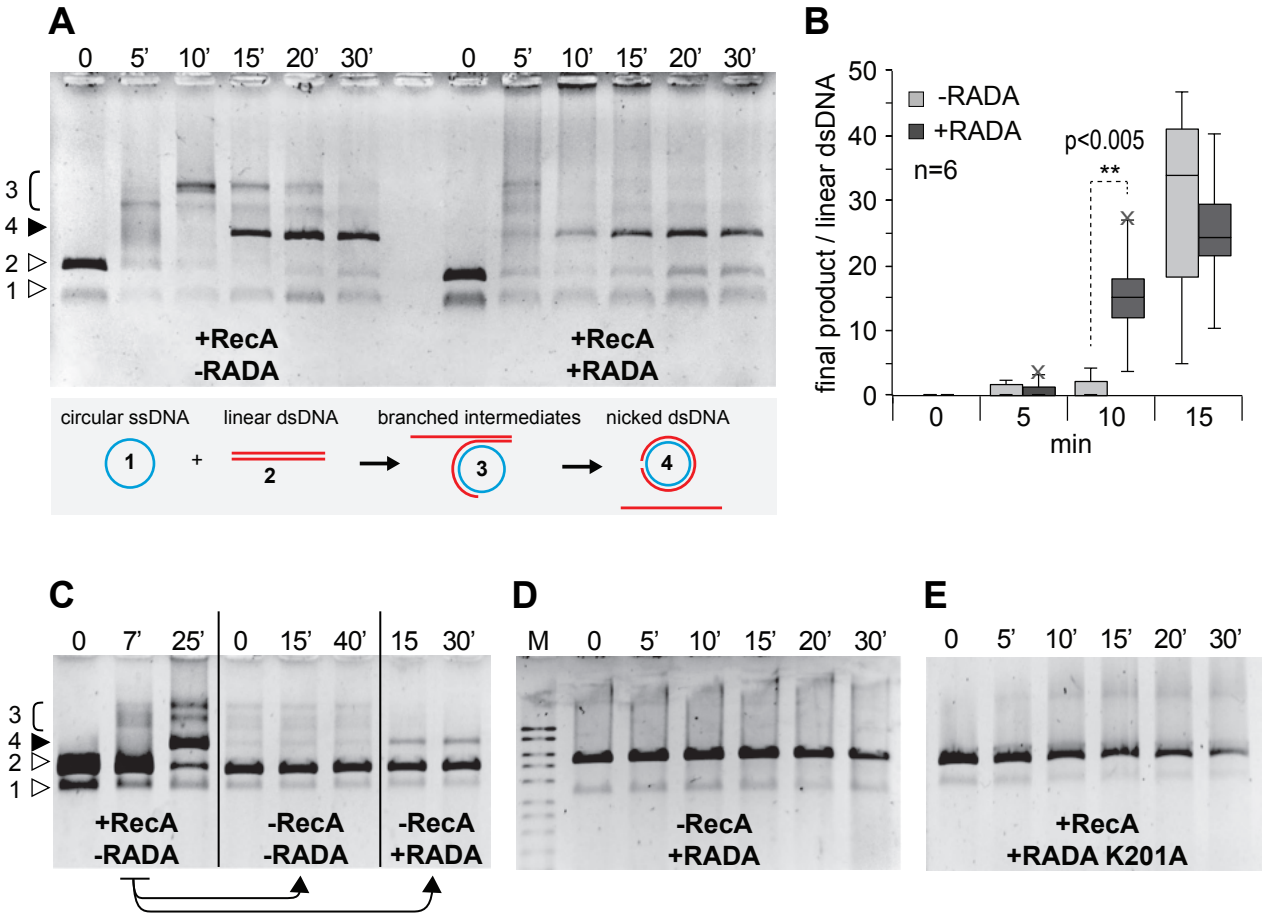

Figure 4. Branch-migration activities of RADA.
(**A**) In an *in vitro* strand-invasion reaction recombinant RADA accelerates branch-migration of DNA heteroduplexes initiated by RecA. An explanation of the different substrates and products is shown. (**B**) Ratio of final product as compared to the initial linear dsDNA substrate in 6 independent experiments, showing that in the presence of RADA there is faster resolution of branched intermediates. (**C**) Experiment showing that RADA alone can finalize branch-migration initiated by RecA: a reaction at t=7 min was arrested by deproteination (left panel) and the DNA purified. Without further addition of RecA or RADA proteins there is no spontaneous progression of the reaction (middle panel), but added RADA can alone resolve the recombination intermediates into the final product (right panel). (**D**) RADA alone cannot initiate strand invasion. (**E**) Mutation of the ATPase Walker domain of RADA (K201A) inhibits the reaction.

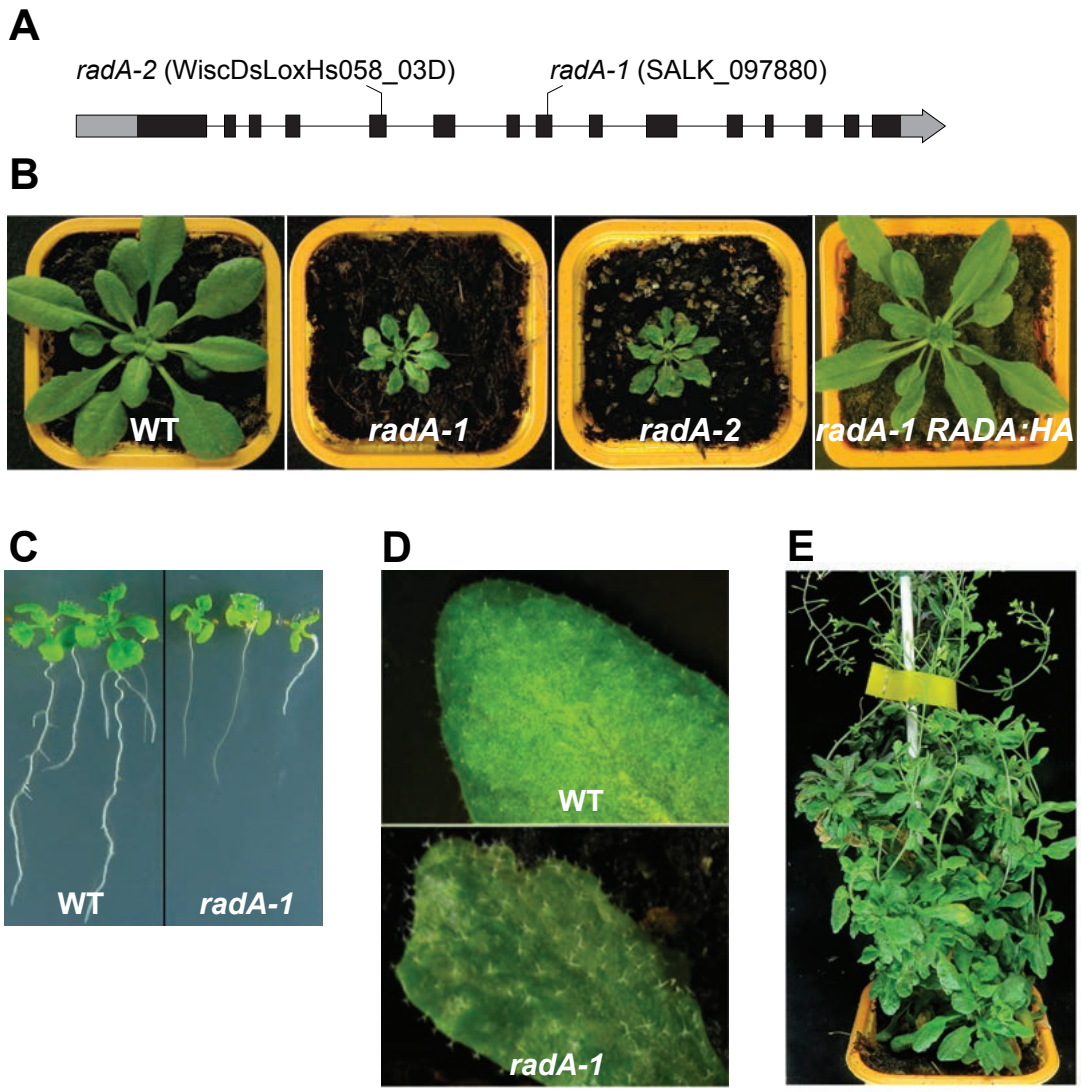

Figure 5. Arabidopsis *radA* mutants and phenotypes.
(**A**) Schematic representation of the Arabidopsis *RADA* gene. Coding sequences are in black and 5'- and 3'-UTRs are in gray. The position of the T-DNA insertions in *radA* mutant lines is shown. (**B**) *radA* plants show severe growth retardation, with distorted leaves presenting chlorotic sectors. These phenotypes can be complemented by expression of HA-tagged RADA (RADA:HA) under control of the endogenous *pRADA* promoter. (**C**) root shortening of *radA* plants. (**D**) Detail of leaf phenotype. (**E**) 4-month old *radA-1* plant grown under short days (8h light), showing perennial vegetative growth with development of aerial rosettes.

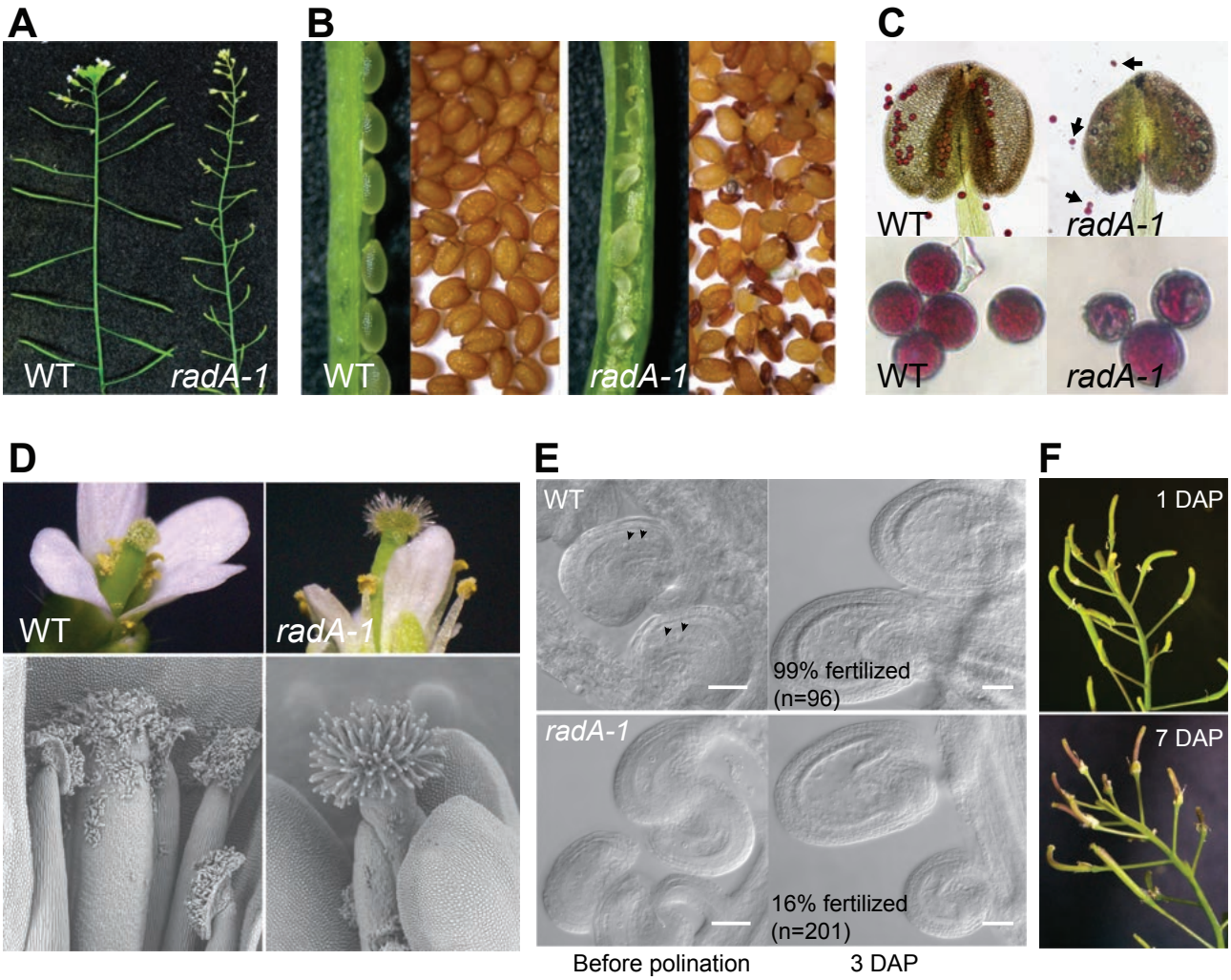

Figure 6. Reduced fertility of *radA* plants.
(**A**) Comparison of WT and *radA* flower stems showing very small *radA* siliques. (**B**) *radA* siliques mostly contain aborted seeds, and most of the few seeds produced are non-viable. (**C**) Alexander staining of pollen in *radA* anthers as compared to WT, showing little pollen production and an abundance of small and aberrant pollen grains (indicated by arrows). (**D**) Visible and SEM Images showing that in *radA* no pollen binds to the papillae of the stigma. (**E**) Differential interference contrast images of ovules on crosses between *radA-1* flowers and WT pollen. Black arrowheads indicate central cell and egg cell nuclei in unfertilized ovules. White arrowheads indicate developing embryos in fertilized ovules, at the 2 up to 8 cells globular stage, three days after pollination (DAP). Only 16 % of *radA* ovules could be fertilized. Scale bar is 50 µm. (**F**) After seven DAP the pollinated pistils of *radA* did not develop further.

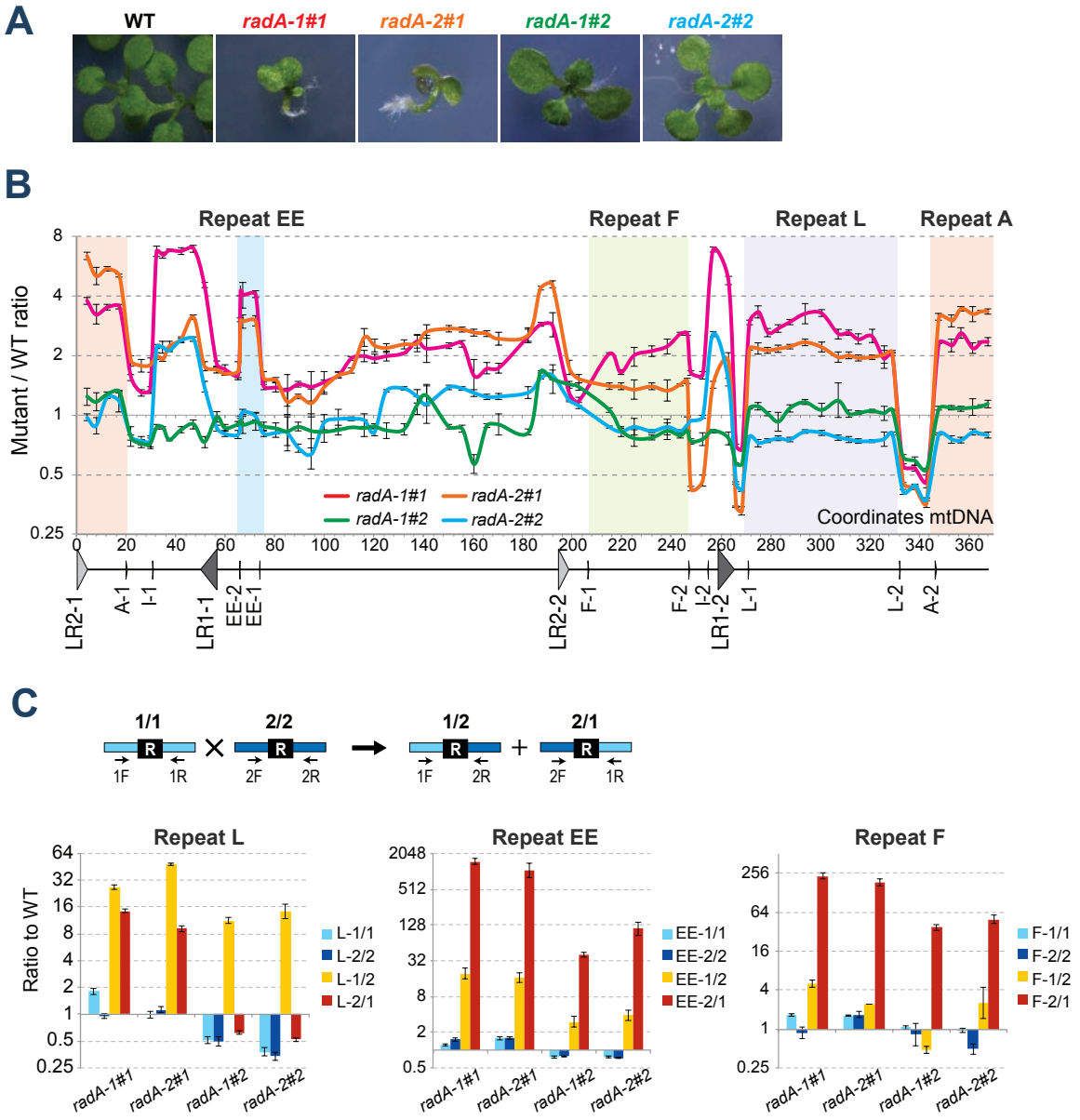

Figure 7. Changes in mtDNA sequences stoichiometry in *radA* mutants because of increased ectopic recombination across repeats.

(**A**) Picture of severely affected (*radA-1*#1 and *radA-2*#1) and mildly affected (*radA-1*#2 and *radA-2*#2) seedlings. (**B**) Scanning of their mtDNA for changes in relative copy numbers of the different mtDNA regions. Sequences spaced 5-10 kb apart on the mtDNA were quantified by qPCR. Coordinates are those of the Col-0 mtDNA sequence. The position of the mtDNA large repeats LR1 and LR2 and of relevant intermediate size repeats are shown below the graphic. Regions with changed stoichiometry flanked by repeat pairs are shadowed. (**C**) Accumulation of crossover products from mtDNA repeats L, F and EE in *radA* seedlings as compared to WT. Results are in a log2 scale. The scheme above shows the qPCR relative quantification of parental sequences 1/1 and 2/2 and of the corresponding crossover products 1/2 and 2/1. Results are the mean of three technical replicates, and error bars correspond to *SD* values.

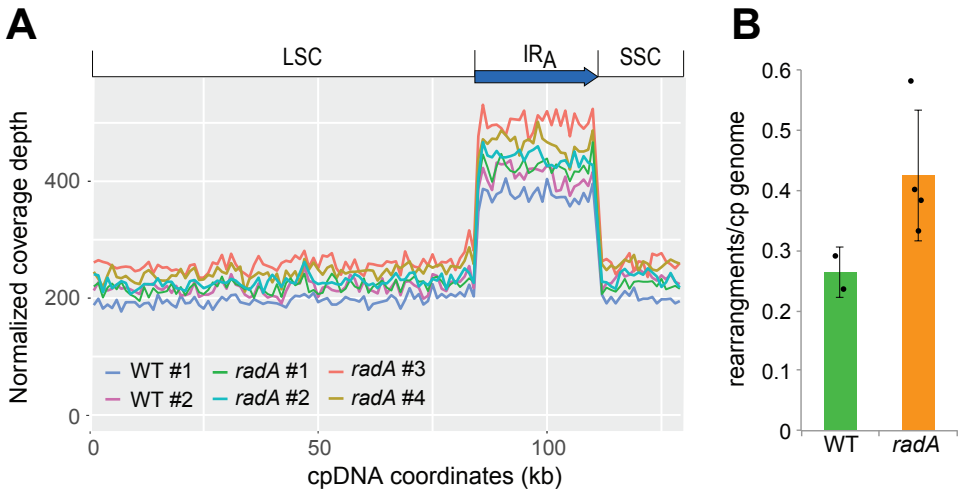

Figure 8. No significant effect of the *radA* mutation on the stability of the plastidial genome.

The DNA from a leaf of four independent 4-week-old *radA-1* plants and of two WT plants was extracted and sequenced on a MySeq Illumina system (2x150 bp paired-end). The reads corresponding to the cpDNA were extracted and investigated for possible changes in cpDNA stability. (**A**) Normalized cpDNA coverage, showing comparable copy number of the cpDNA in WT and in *radA*, and no apparent changes in sequences stoichiometry. A schematic representation of the cpDNA is shown above, indicating the large and small single-copy regions (LSC and SSC, respectively) and a single copy of the inverted repeated region (IR). (**B**) Abundance of reads identified as corresponding to rearranged cpDNA molecules (see supplemental figure 7 for a scheme of the analysis pipeline). A slight increase, up to two-fold as compared to WT, was identified in the *radA* plants.

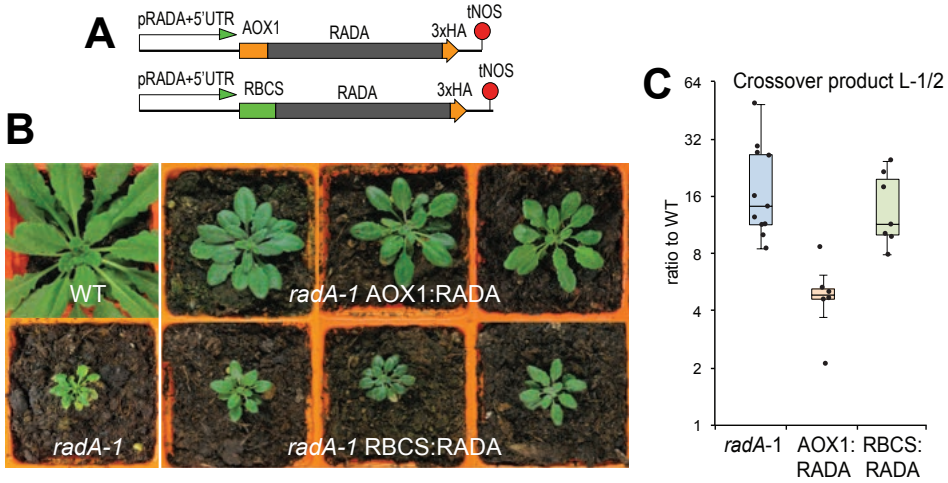

Figure 9. Hemicomplementation of *radA*

(**A**) Schematic representation of the constructs used for testing hemicomplementation of the *radA* phenotypes, with a construct only targeting RADA to mitochondria, by fusion to the targeting sequence of alternative oxidase (AOX1) and with a construct only targeting RADA to plastids, by fusion to the targeting sequence of the small subunit of Rubisco (RBCS). (**B**) Growth phenotypes of four-week-old hemicomplemented plants in a segregating T2 population as compared to WT and *radA-1*. Only partial complementation was observed with the AOX1:RADA construct, but plants complemented with the RBCS:RADA construct showed little or no complementation. (**C**) Relative quantification of the accumulation of crossover product L-1/2, resulting from ectopic recombination involving mitochondrial pair of repeats L in *radA-1* and in hemicomplemented plants (log2 scale).

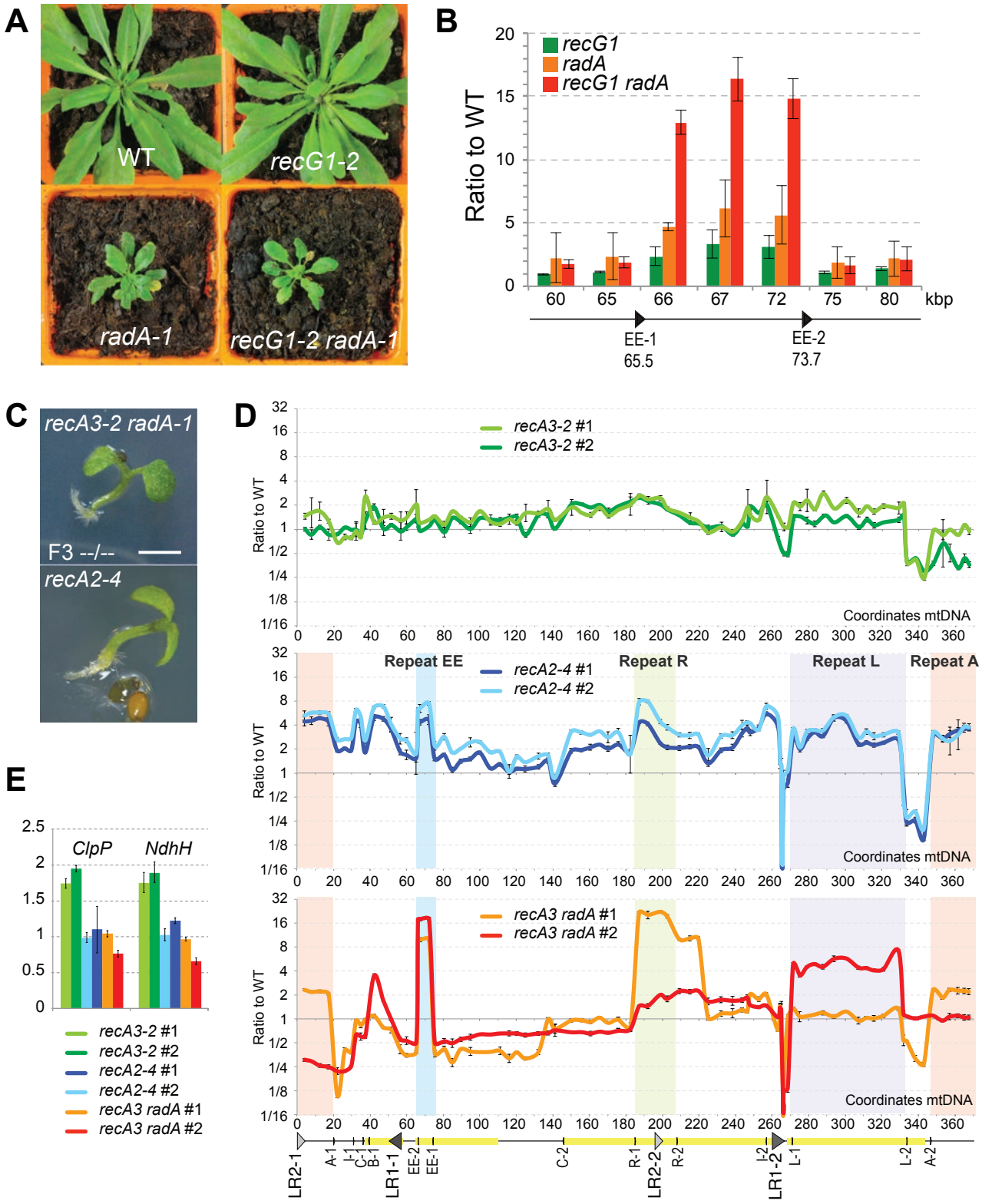

Figure 10. Synergistic effects of the *radA* mutation on *recG1* and *recA3*.
(**A**) Crosses of *recG1-2* and *radA-1* (pollen donor) show that double homozygote *recG1 radA* plants are not more affected in their development than simple homozygote *radA* plants. (**B**) qPCR analysis of the copy number of mtDNA sequences around and within the region comprised between the pair of repeats EE, previously shown to generate an episome by recombination in *recG1* plants (Wallet et al., 2015). Autonomous replication of the episome is significantly increased in the *recG1 radA* double mutant. Results show the mean and *SD* error bars from 2 or 3 (for *recG1 radA*) biological replicates. (**C**) Double homozygote *recA3 radA* seedlings do not grow roots and do not grow further. The phenotype is similar to the one observed for *recA2* mutants (Miller-Messmer et al., 2012). The scale bar is 1 mm. (**D**) Scanning of the copy numbers of the different mtDNA regions, as described in Figure 7, in pools of *recA3 radA* double mutant seedlings. Results were compared to those of WT seedling of same size, and are represented in log scale. Sequences that are also present in the nuclear genome of Col-0 are shaded yellow in the mtDNA representation.

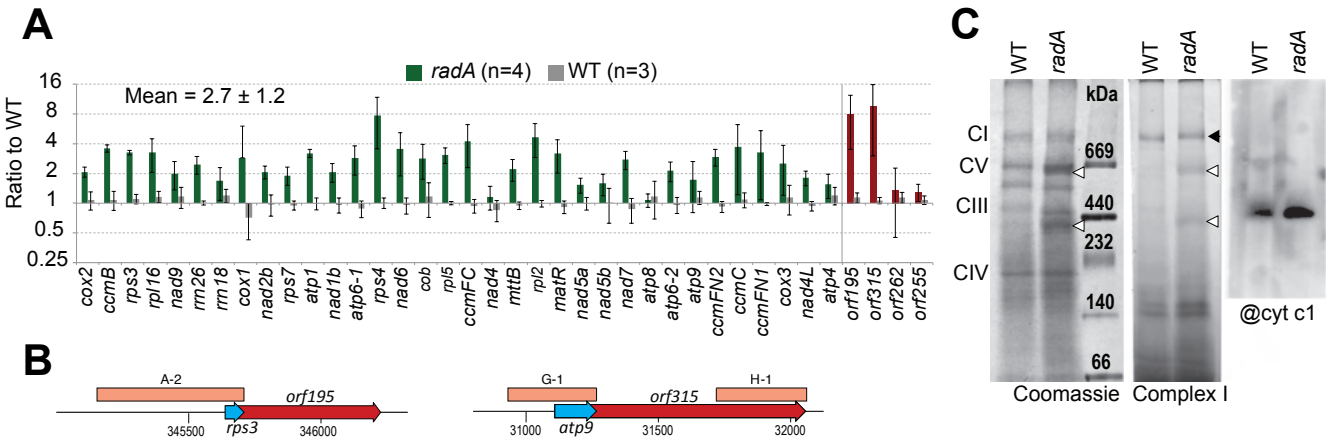

Figure 11. Accumulation of mitochondrial transcripts in *radA*.
(A) Representative mitochondrial transcripts were quantified by RT-qPCR, from the RNA of 10-day-old seedlings grown *in vitro,* and normalized against a set of nuclear housekeeping genes. The quantification of several orf transcripts whose expression could be potentially affected by ectopic recombination involving IRs is shown on the right, in red. Results are on a log2 scale and are the mean from four biological replicates (two pools of *radA-1* and two pools of *radA-2* seedlings) with the corresponding *SD* error bars. **(B)** Chimeric *orf195* and *orf315* created by recombination whose transcription is augmented in *radA* plants. The regions corresponding to *rps3* and *atp9* sequences are shown in blue. Repeated sequences are represented by orange bars. Coordinates on the mtDNA are indicated. (**C**) Blue-Native gel analysis of WT and *radA* purified mitochondria. 80 µg of proteins were loaded in each well, and run in parallel with size markers (High Molecular Weight Calibration Kit, GE Healthcare). Coomassie staining, complex I activity staining and immunodetection of complex III (with a cytochrome c1-specific antibody) revealed no apparent changes in *radA* respiratory complexes. The white arrowheads indicate green-yellow bands that were already visible before staining and likely corresponded to plastidial contamination. The black arrowhead indicates the complex I activity band.

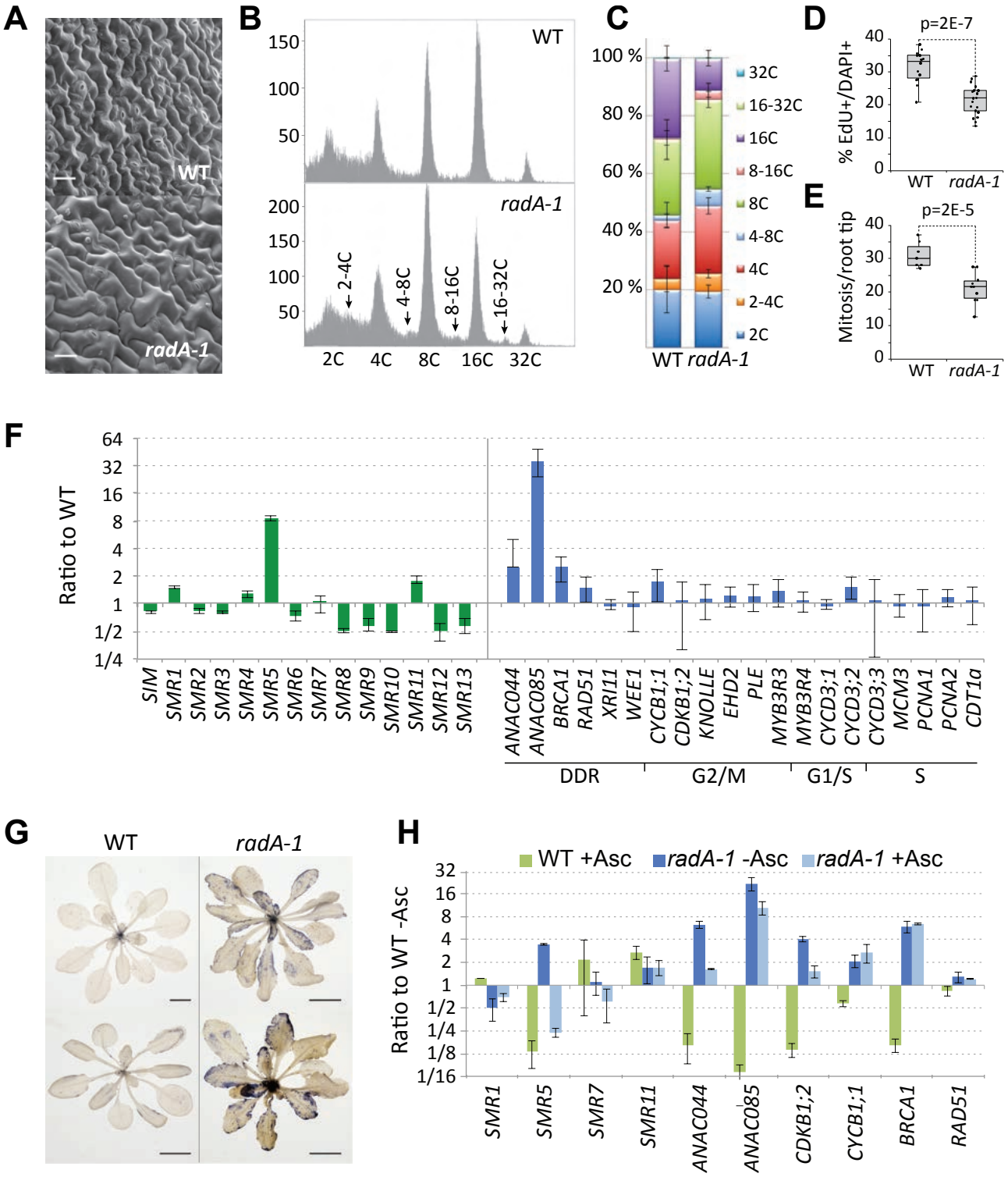

Figure 12. Cell cycle progression is impaired in *radA* plants.
(A) Scanning electron microscopy images showing much larger epidermal cells and fewer stomata in *radA* leaves. Scale bar is 20 µm. **(B)** Flow-cytometry profiles obtained in WT (Col-0) and *radA.* The DNA content of nuclei extracted from the first true leaves of 20-day-old plants was analyzed. **(C)** Ploidy distribution, showing decreased endoreduplication in the mutant, with an increased proportion of 4C and 8C nuclei and a decreased proportion of 16C nuclei. Values are the average ± *SD* of 4 experiments for WT and six experiments for *radA* (n>20 000 nuclei). **(D)** Decreased DNA synthesis in the nuclei of *radA* root tip cells, as evaluated by the ratio between EdU positive and DAPI (4',6'-diamidino-2-phénylindol) positive cells. **(E)** Decreased number of cells undergoing mitosis. Significances were calculated by Student's t test. **(F)** RT-qPCR analysis of the expression of a set of cell cycle related genes in 10-day-old WT and *radA* seedlings, revealing significant activation of *SMR5* and *ANAC085*. The data is represented in a log2 scale and is the mean ± *SD* of three biological replicates (two pools of seedlings from *radA-1* and one from *radA-2*). **(G)** NBT (nitro blue tetrazolium) staining for O^{2-} in plants of equivalent size grown under the same conditions, showing that *radA* mutants accumulate much more ROS than WT plants. Scale bar is 1 cm. **(H)** The expression of several cell cycle-related genes is suppressed by the ROS quencher ascorbic acid (1 mM), both in WT and in *radA* 10-day-old seedlings.

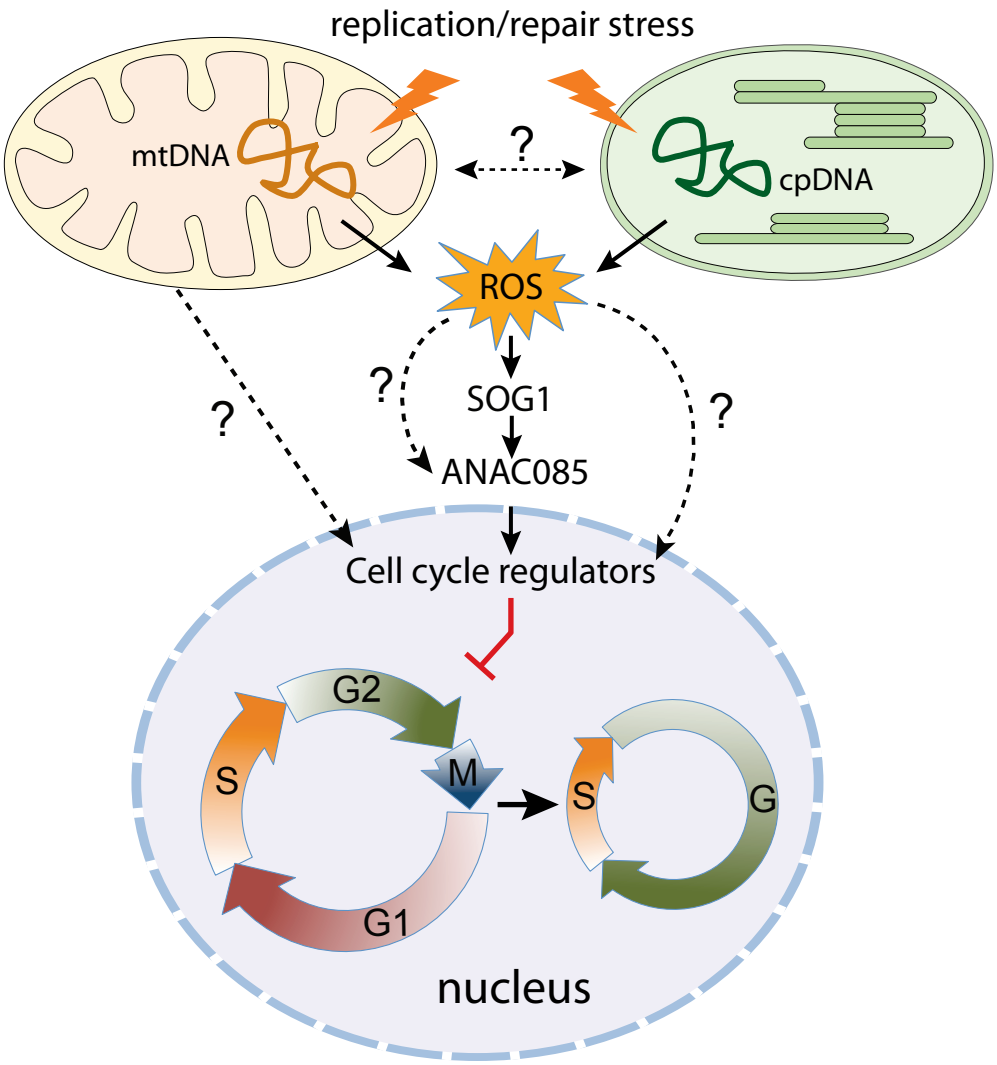

Figure 13. Model for possible retrograde regulation by organellar DNA instability

Possible retrograde effect of the instability of organellar genomes on the expression of cel- cycle regulators inhibiting plant growth and development. The release of ROS from mitochondria and/or chloroplast could be the signal transmitted to the nucleus.